Extraction of Technetium-99m

Using a Two-Phase Flow in a Microchannel

A.R. Blok

Technische Universiteit Delft

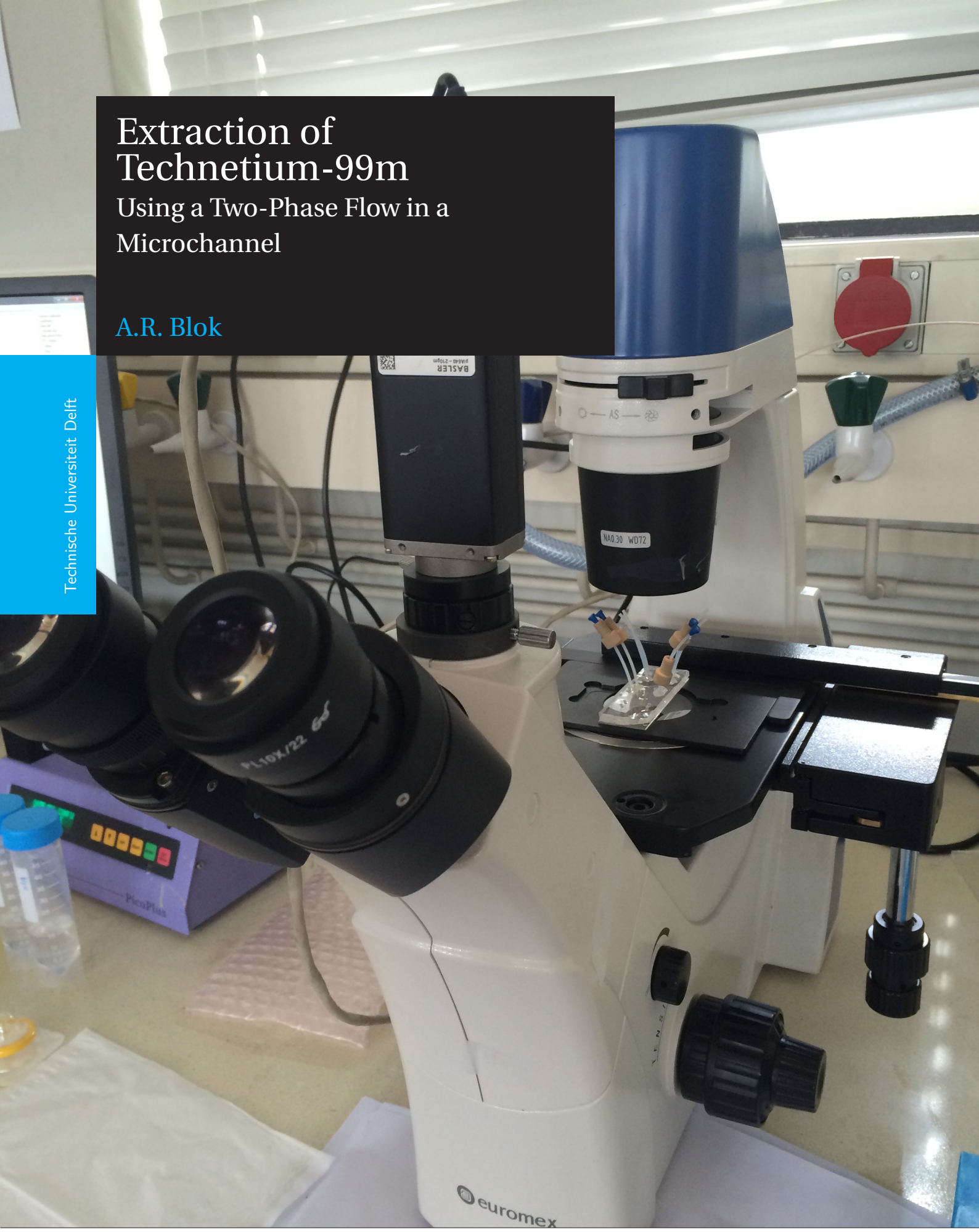

TU Delft Delft University of Technology

Challenge the future

EXTRACTION OF TECHNETIUM-99M

USING A TWO-PHASE FLOW IN A MICROCHANNEL

by

A.R. Blok

in partial fulfillment of the requirements for the degree of

Bachelor of Science
in Applied Physics

at the University of Technology Delft,
to be defended publicly on Thursday July 9, 2015 at 13:30.

Supervisor:	Dr. ir. M. Rohde	
Thesis committee:	Dr. ir. M. Rohde,	TU Delft
	Dr. ir. E. Oehlke,	TU Delft
	Prof. dr. ir. J. Derksen	TU Delft

An electronic version of this thesis is available at http://www.nera.rst.tudelft.nl.

TU Delft Delft University of Technology

NOMENCLATURE

Symbol	*Description*
A	Area
α	Correction factor
c	Concentration
C	Compactness
D	Diffusion coefficient
G	Gibbs free energy
γ	Interfacial tension
h	Channel height
k_b	Boltzmann constant
K_D	Distribution coefficient
L	Channel length
L_{ext}	Extraction length (maximum channel length)
μ	Viscosity
$\phi_m^{''}$	Mass flux
N	Grid length
P	Wetted perimeter
Δp_{lap}	Laplace pressure
Δp_{hyd}	Hydrodynamic pressure difference
Q	Flow rate
R	Radius
R	Universal gas constant
R_{hyd}	Hydraulic resistance
σ_A	Diameter molecule A
T	Temperature
t	Time
Δt	Time step
τ	Time scale
θ_{con}	Contact angle
θ_{re}	Receding contact angle
θ_{ad}	Advancing contact angle
V	Velocity
w	Width
x	x-Coordinate in the channel

ABSTRACT

This thesis describes the research done on a microfluidic extractor used for the extraction of technetium-99m. The extractor is based on a two-phase parallel flow with a stable liquid-liquid interface. Within this system a molybdenum solution containing the technetium compound pertechnetate (TcO_4^-) is used as one of the phases. The technetium compound is extracted to 2-butanone in the other phase.

To establish a successful and efficient extraction, multiple features have to be taken into account. First of all, the geometrical properties of the extractor influence the stability of the interface and the extraction efficiency. Stability of the interface means that the interface is located in the middle of the channel and is not disrupted. The efficiency of the extractor is taken as the the amount of pertechentate that is extracted from the molybdenum solution compared to the amount of pertechentate left in the molybdenum solution.

Furthermore, the chemical properties of the substances present in the system, such as the viscosity of the solutions, the interfacial tension, the diffusion coefficients and the distribution coefficient, have an effect on the operation and efficiency of the extractor.

It is a challenge to find the right combination of all these parameters resulting in an efficient extraction of the desired chemical entity. The goal of this research is to obtain an accurate simulation model for the extraction process of technetium-99m and find the optimized parameters for the geometrical design of the microfluidic platform to establish the highest possible extraction efficiency.

For this reason, a numerical model for the diffusion process is created. Beside this, the forces acting on the flow in the channel are studied. The force balance determines the stability of the interface. The force balance exists of the hydrodynamic pressure difference and the Laplace pressure. The hydrodynamic pressure difference accounts for the viscosity and flow rates of the fluids. The Laplace pressure is initiated by the surface tensions of the phases. From the force balance an expression for the maximum extraction length (L_{ext}) for the channel is derived. An analytically obtained result for an optimized extraction length has been reported by Goyal and Desai in 2013 [1]. Their expression was adjusted to account for a two-phase flow instead of a one-phase flow. Furthermore, a miscalculation was detected in their derivation. A new expression for the maximized extraction length is used for further calculations.

For all analysis, calculations were performed for a channel width ranging from 10-100μm, a channel height ranging from 10-100μm and flow rates ranging from 10-100μL/min. From the calculations on the force balance it could be concluded that a larger channel width and height results in a longer maximal extraction length. Furthermore, the extraction length is longer for lower flow rates. The diffusion model was used for the optimization process. First, the optimal extraction lengths were calculated for the widths, heights and flow rates whitin the given ranges. Next, the contact time was derived from the optimal extraction length and flow rate. The contact time and width were used to calculate the amount of diffused pertechentate through the interface. Finally, the extraction efficiency is calculated. The optimization is conducted for four test cases, namely:

1. To obtain the highest extraction efficiency possible, what are the corresponding geometrical parameters and flow rate?

2. If the extraction length is limited by the chips dimensions, take $L_{ext} < 0.01m$. What is the maximum extraction efficiency that can be reached?

3. What is the extraction efficiency under the conditions $L_{ext} < 0.01m$ and the lower limit of the flow rate range is increased to 20μL/min?

4. What efficiency can be reached when our system is limited to a channel height of 50μm. For this test case the conditions proposed before still apply.

The first test case resulted in an extraction efficiency of 99% and an extraction length of 12.0 cm. For the second test case an extraction efficiency of 64% and extraction length of 8.09 mm was obtained. The third test case resulted in an extraction efficiency of 44% and an extraction length of 9.41 mm. Finally, the fourth test case resulted in an extraction efficiency of 27% and an extraction length of 8.68 mm.

It can be concluded that the extraction efficiency, for extraction lengths that fit on a micro chip, are significantly lower compared to the extraction efficiency obtained in the first test case. Furthermore, the limitations on the flow rate and channel height have a negative influence on the extraction efficiency. Consequently, ideas for improvement and further research are proposed that can possibly increase the extraction efficiency for this system.

Furthermore, it was experimentally determined whether the combination of a molybdenum solution and 2-butanone results in a proper two-phase immiscible flow. A stable flow profile was obtained for a flow rate of 20μL/min.

CONTENTS

1

INTRODUCTION

This thesis describes the research done on a microfluidic extractor system used for the extraction of technetium-99m. The extractor is based on a two-phase parallel flow with a stable liquid-liquid interface. Previous studies have shown promising results concerning the efficiency of micro-extractor system used for multiple extraction processes. One of these studies, conducted by Goyal and Desai, was published in 2014.[1] This study reported an extraction efficiency exceeding 95% for the extraction of radioactive copper (Cu-64) using a microfluidic liquid-liquid extraction platform. Extraction of a chemical entity from one phase to the other takes place by diffusion through the liquid-liquid interface. This chapter gives an introduction to the research subject and formulates the research question. First, paragraph 1.1 describes the idea and applications of lab-on-chip systems. Then, paragraph 1.2 explains the design and working of the extractor. In paragraph 1.3, the motivation for this study is explained and a research question is formulated. Paragraph 1.4 describes the research methods that are used. Finally, paragraph 1.5 gives the outline for this thesis.

1.1. LAB ON CHIP

A lab-on-chip system can be thought of as the shrinking of a large scale laboratory to a chip. A chip can contain multiple subsystems, such as mixers, reactors, separators and extractors. The chips are used in applications where only small volumes of reagents are available or needed. Lab-on-chip technology is applied in e.g. biotechnology, pharmacology, medical diagnostics and chemical research. The small volumes, ranging from picoliters to nanoliters, allow for fast analysis. The chips are compact, portable systems with the potential for cheap mass production.[2] The chips are approximately 2 by 5 cm and the channels have a width of 50-100 μm. Figure 1.1 gives an impression of the lab-on-chip technology and the size of the chip.

The main function of a lab-on-chip system is to handle fluids. A fluid is either a gas or a liquid and is characterized by the property that it will deform under the action of external forces. The influence of forces at fluids differ at microscale compared to macroscale. The dimensionless *Bond* number, formulated in equation 1.1, gives the gravity-to-surface tension ratio.[5]

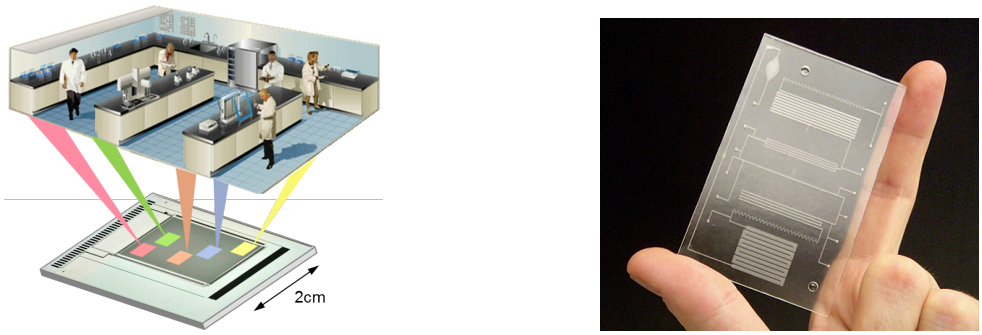

Figure 1.1: The left picture illustrates the downscaling of a complete laboratory to a chip.[3] In the right picture an example is given of a chip containing multiple subsystems. [4]

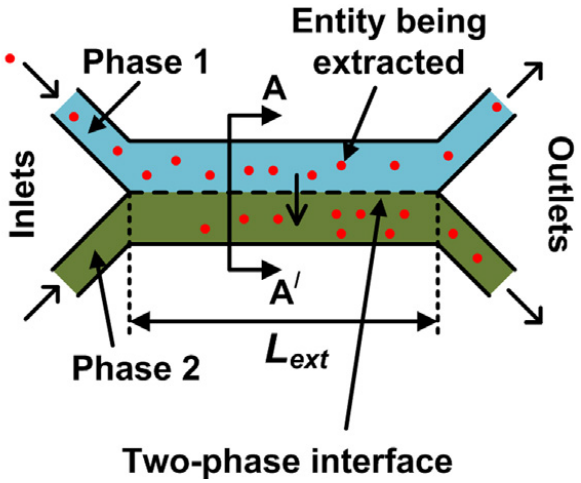

Figure 1.2: A schematic illustration of the extractor. The aqueous solution is represented with the blue phase and the organic solution with the green phase. The red dots illustrate the extracted species. The length of the main channel is called the extraction length L_{ext}. [1]

$$Bo = \frac{\Delta\rho g L^2}{\sigma} \tag{1.1}$$

Here, $\Delta\rho$ is the density difference between two phases, g is the gravitational acceleration. L is a characteristic length and σ is the surface tension. The Bond number indicates whether a system is dominated by buoyancy or surface tension forces. For micro-systems, a small Bond number applies and surface tension plays a much more dominant role than gravitational forces. Furthermore, the gravity-to-viscosity ratio can be analyzed using the dimensionless number of *Grashof*. The Grashof number is formulated in equation 1.2[5].

$$Gr = \frac{gL^3\rho}{\mu^2}\Delta\rho \tag{1.2}$$

Here, $\Delta\rho$ is the density difference between two phases, g is the gravitational acceleration. L is a characteristic length and μ is the dynamic viscosity. For microfluidic systems the Grashof number is low. Hence, the viscous force has a more dominant influence than the gravitational force. The influences of different forces on the fluids have to be taken into account when doing calculations on the fluid flow. In paragraph 2 this is further explained.

1.2. THE EXTRACTOR

In this research the extractor is of interest. The extractor is based on a two-phase parallel flow in a microchannel with a liquid-liquid interface. Hence, the two phases must be immiscible. Up and till now, most chips are made out of glass or silicon due to their compatibility with organic solvents. However, an extensive fabrication process is needed for the production of the chips when these materials are used. Research is done on the use of polymer-based microfluidic platforms and shows promising results.[1] The fabrication of polymer-based chips, asks for a less involved fabrication process and the chips are still compatible with most organic solvents.

For this research an extractor made out of polydimethylsiloxane (PDMS) is studied. PDMS is a silicon-based organic polymer. It is highly hydrophobic and has a contact angle of approximatly 108°with water.[6] As organic solvent 2-butanone is used, also known as ethyl methyl ketone (MEK). The aqueous phase consists of a molybdenum solution containing the technetium compound pertechnetate (TcO_4^-). This compound is extracted to 2-butanone. Figure 1.2 shows a schematic illustration of an extractor. Each phase has its own inlet and outlet channel. In the middle of the main channel a liquid-liquid interface exists. The red dots represent a chemical entity that is extracted from phase 1 to phase 2. The blue phase consists of the aqueous solution, the green phase represents the organic solution.

The extractor operates under a pressure difference applied over the inlet and outlet channel of the phases. Herefore, two pumps are connected to the inlets of the extractor. The outlets are exposed to atmospheric pressure. The flow rates in both phases can be varied by the pumps. Furthermore, for a rectangular shaped

channel, the width and height can be varied. Previous research has reported flow rates withing the rang of 20 μL/min to 100 μL/min, widths within the range of 20 μm to 100 μm and heights of 50 μm to 100 μm, to give a high extraction efficiency.[1] However, the geometrical parameters and the flow rates are not universal applicable. Depending on the chemical characteristics of the substances used in the system, other values for the parameters might give better results.

The extraction process is based on diffusion of the chemical entity from phase 1 to phase 2. Herefore, it is important to choose the organic solution such that the solubility of the chemical entity is higher in the organic phase than in the aqueous phase. It is also possible to use actively extracting molecules in the organic phase that form complexes with the extracted species at the interface. Consequently, less contact time is needed between both phases and the technique can result in a higher extraction efficiency.

1.3. RESEARCH QUESTION

To establish a successful and efficient extraction, multiple features have to be taken into account. First of all, the geometrical properties of the extractor influence the stability of the interface and the extraction efficiency. Stability of the interface, means that the interface is located in the middle of the channel and is not disrupted. The efficiency of the extractor is a measure for the amount of pertechnetate that is extracted from the molybdenum solution compared to the amount of pertechnetate left over in the molybdenum solution.

Furthermore, the chemical properties of the substances used as solvents and solutes have an effect on the operation of the extractor. It is a challenge to find the right combination of all these parameters resulting in an efficient extraction of the desired chemical entity.

As mentioned in the previous paragraph, earlier studies have reported results concerning the extraction efficiency of a microfluidic extractor. These results are based on analytic solutions for a simplified diffusion model. Namely, the extraction process is defined as a diffusion limited process only in the first phase (the aqueous phase), with zero concentration at the interface. This simplification was justified by the fact that in their study an active extractant is used in the second phase to form complexes with the extracted species at the interface. The concentration of extractant was taken six times higher than that of the extracted species. Hence, they assumed the concentration of the extracted species to be zero at the interface due to the immediate complex-formation reaction with the extractant[1].

In the extractor studied in this research there is no active extractant involved in the extraction process, thus the simplified diffusion model is not applicable to our situation. To be able to analyze the extraction process of the technetium-99m compounds a more complex diffusion model has to be used. Based on this analysis the geometrical parameters for the microfluidic platform should be chosen and combined in such a way a stable interface is maintained and a high extraction efficiency is established. Hence, the research question for this thesis can be formulated as follows:

What is an accurate simulation model for the extraction process of technetium-99m and what are the optimized parameters for the geometrical design of the microfluidic platform to establish the highest possible extraction efficiency?

To answer this question, the physics of diffusion will be studied. Hereby, transient mass transport through an interface of a two-phase system must be taken into account. Furthermore, forces applied to the two-phase flow, influencing the stability of the interface, will be analyzed. The research methods used for the study are outlined in paragraph 1.4 *Methodology*.

1.4. METHODOLOGY

To find an answer to the research question both qualitative and quantitative research is done. First, literature is studied to gain insight in the physics behind the extraction process. The result of this literature study is presented in part I. The literature that is used is listed in chapter 7 *Bibliography*.

For the simulation of the diffusion process a numerical approach is used. The calculations and simulations are done in MATLAB. Based on the results of the simulations, optimized parameters for the geometrical design of the microfluidic platform are determined. Furthermore, experimental research is done to study the flow of the two-phase system. This is followed by the analysis wherein the results are presented. Finally, conclusions are drawn and recommendations are presented for further research.

1.5. REPORT STRUCTURE

The report is structured in three parts:

Part I Theory

This part contains the theory that is used to create a numerical model as described in part II. Chapter 2 describes the force balance present at the interface of the two-phase parallel flow in the microchannel. In Chapter 3 the phenomena diffusion is explained. Here, Fick's law is clarified and mass transport through an interface is analyzed.

Part II Analysis

This part consists of two chapters. Chapter 4 explains for both the numerical simulation and the experimental simulation, how the simulations are conducted and what parameters were used. Chapter 5 presents the results for the numerical and experimental simulations.

Part III Evaluation

In this part the results are evaluated. In chapter 6 the conclusions for this research are presented. In chapter 7 possible improvements for this research are discussed and ideas for future research are proposed.

I

THEORY

2

MICROCHANNEL FORCE BALANCE

As described in chapter 1 a microfluidic platform can be used for liquid-liquid extraction. In this chapter the force interaction within the microchannel is explained. In paragraph 1.2 is mentioned that the geometrical parameters of the extractor and the chosen flow rates influence the extraction results. Furthermore, the chemical characteristics of the substances in the system, such as viscosity, diffusion coefficients and surface tensions, influence the behaviour of the flow.

In the microchannel, for the flow rates and widths as mentioned in paragraph 1.2, both phases experience a laminar flow with a Reynolds number of approximately 10^{-7}. As explained in paragraph 1.1 surface tension and viscosity have a dominant influence on the flow pattern at microscale. These forces arise due to interfacial tension at the interface and due to the flow rate and resistance of both fluids. A proper balance of these forces will result in a stable interface, this means that the interface does not break or shift toward one of the channel walls. Figure 2 shows a schematic illustration of the cross section of the channel illustrated in figure 1.2. In the picture the forces, due to interfacial tension and the combination of the flow rate and resistance, are denoted by $\Delta P_{laplace}$ and ΔP_{flow} respectively.
Throughout the channel the pressures form a balance as formulated in equation 2.1.

$$\Delta p_{laplace} + \Delta p_{hyd} = 0 \tag{2.1}$$

In the upcoming paragraphs expressions for $\Delta p_{laplace}$ and Δp_{hyd} are derived. In paragraph 2.1 the influence of the flow rate and resistance on the flow is explained. Paragraph 2.2 describes the relation between the interface curvature and interfacial tension. Finally, in paragraph 2.3 a general expression for the maximum extraction length is formulated.

2.1. HYDRODYNAMIC PRESSURE

As both solutions flow through the channel, the resistance in the phases causes energy to dissipate. The resistance depends on the dynamic viscosity and the cross section of the flow. Due to different viscosity's, each phase will experience a different resistance. Consequently, a pressure drop will occur over each phase. This pressure drop also depends on the flow rate, a general expression for the pressure drop is formulated in equation 2.2.

$$p_{hyd} = QR_{hyd} + p_{out} \tag{2.2}$$

Here, Q denotes the flow rate in $(\frac{m^3}{s})$, R the hydraulic resistance, in $(\frac{kg}{m^4 s})$, over a length L and p_{out} is the pressure at the outlet of the channel. There is need for a general resistance expression which can be used in the case of complex cross sections. To obtain this expression a correction must be made on the commonly used resistance term for channels with a circular cross section. Herefor, a dimensionless geometrical correction factor is introduced, expressed by α. [7]

$$\alpha = \frac{R_{hyd}}{R^{\star}_{hyd}} \tag{2.3}$$

With $R^{\star}_{hyd}$ given by equation 2.4.

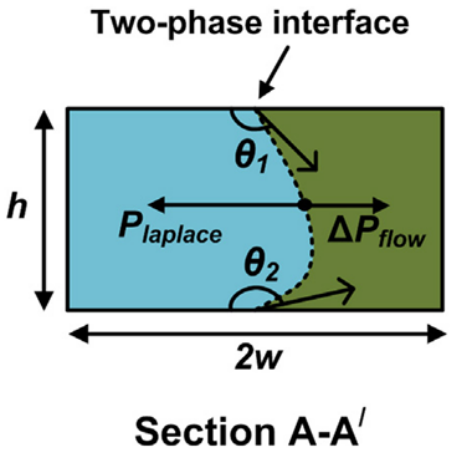

Figure 2.1: A schematic illustration of the cross section of the extractor. The aqueous solution is represented with the blue phase and the organic solution with the green phase. In the picture the forces due to interfacial tension and the combination of flow rate and resistance are denoted by $\Delta P_{laplace}$ and ΔP_{flow} respectively. ΔP_{flow} will be denoted by ΔP_{hyd} throughout the rest of the text. Furthermore, h represents the height and w the half-width of the channel.[1]

$$R^{\star}_{hyd} = \frac{\mu L}{A^2} \tag{2.4}$$

Here, μ is the dynamic viscosity of the fluid, L is the extraction channel length and the area of the cross section. For this research, the cross section of the extraction channel is assumed to be rectangular. The correction factor for rectangular shaped cross sections α can be derived analytically. The result is shown in equation 2.5.[8]

$$\alpha(C) = \frac{22}{7}C - \frac{65}{3} \tag{2.5}$$

Here, C represents the *compactness* which is a dimensionless number defined by the ratio between the wetted perimeter and the cross section of the fluid flow.

$$C = \frac{P^2}{A} \tag{2.6}$$

For each phase in the extractor the wetted perimeter is equal to $2w+h$, with w the half-width and h the height of the channel. Hereby, the friction of the liquid-liquid interface is neglected under the assumption that both fluids flow in the same direction and the flow rates do not differ to a great extend. Substituting the expression for the compactness in equation 2.5 gives the correction factor applicable for the geometry of the extractor studied in this research. This expression is formulated in equation 2.7.

$$\alpha = \frac{22}{7}\frac{(2w+h)^2}{wh} - \frac{65}{3} \tag{2.7}$$

Substitution of equation 2.7 in equation 2.4 and rewriting the result to an expression for R_{hyd} results in equation 2.8.

$$R_{hyd} = \frac{\mu L}{(wh)^2}\left(\frac{22}{7}\frac{(2w+h)^2}{wh} - \frac{65}{3}\right) \tag{2.8}$$

Multiplying equation 2.8 with the flow rate will give the pressure drop over a channel length L. Now, it is interesting to obtain an expression for the pressure difference between both phases which is a consequence of the difference in pressure drop over each phase. Combining equation 2.2, 2.7 and 2.8 gives an expression for the pressure difference obtained over a length L. This pressure difference is called the hydrodynamic pressure difference Δp_{hyd} and is formulated in equation 2.9.

$$\Delta p_{hyd} = \frac{\alpha L}{(wh)^2}(\mu_{aq}Q_{aq} - \mu_{org}Q_{org}) + \Delta p_{out} \tag{2.9}$$

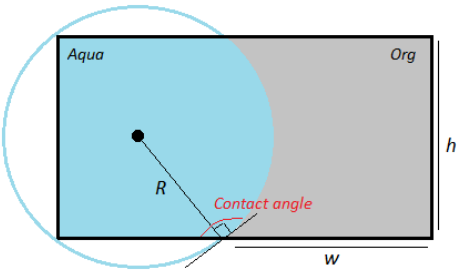

Figure 2.2: A schematic illustration of the cross section of the extractor. The contact angle is denoted in red. Furthermore, h represents the height and w the half-width of the channel. Made by A. Blok

The pressure balance, formulated in equation 2.1, can now be expressed using the expression for Δp_{hyd} from equation 2.9. In the next paragraph an expression for the Laplace pressure is derived.

2.2. YOUNG-LAPLACE EQUATION

As explained in paragraph 2.1 a pressure difference is present between the phases in the extraction channel. This pressure difference is balanced by the Laplace pressure. The Laplace pressure is a pressure difference that is initiated by curving the interface between the fluids. The relation between the Laplace pressure and the curvature of the interface is formulated in equation 2.10, the *Young-Laplace equation.*[9].

$$\Delta p_{laplace} = \gamma(\frac{1}{R_1} + \frac{1}{R_2}) \tag{2.10}$$

Here, γ denotes the interfacial tension between the phases, R_1 and R_2 represent the principal radii of curvature. For the interface in the extractor the radii of curvature are vertical and parallel to the liquids flow direction. Hence, $R_1 = R$ and $R_2 = \infty$ respectively. The expression for the Laplace pressure reduces to equation 2.11.

$$\Delta p_{laplace} = \gamma(\frac{1}{R}) \tag{2.11}$$

Figure 2.2 shows the cross section of an extraction channel where the interface is assumed to be part of a perfect circle. The interface has radius R, the channel height is depicted by h. The contact angle depends on the material the channel is made of and on both solutions. The hydrodynamic pressure difference changes over the length of the channel. Meanwhile, the contact angle adjusts to these changes to form a new pressure balance. The maximum and minimum contact angle that is accepted by the interface, is denoted by the *advancing contact angle* and the *receding contact angle* respectively. These angels are also determined by the chemical properties of the system. Equation 2.11 can be rewritten in terms of the contact angle and the height of the channel.

$$\Delta p_{laplace} = \frac{2\gamma \sin(\theta_{con} - 90°)}{h} \tag{2.12}$$

The hydrodynamic pressure difference is thus limited by the advancing and receding contact angle.[10]

$$\frac{2\gamma \sin(\theta_{re} - 90°)}{h} < \Delta p_{hyd} < \frac{2\gamma \sin(\theta_{ad} - 90°)}{h} \tag{2.13}$$

When the hydrodynamic pressure difference exceeds the minimum or maximum Laplace pressure, the organic phase moves toward the aqueous phase or visa verse. This is illustrated in figure 2.3.

The Laplace pressure is defined by values for the parameters specific to the system studied in this research. At 25°, water has a surface tension of 72,8 mN/m. 2-Butanone has a much lower surface tension of 24,6 mN/m.[11] Furthermore, the channel is highly hydrophobic. Consequently, the interface between the aqueous and 2-butanone solution has a curvature pointed in the direction of the organic phase, as is shown in figure 2.2. The advancing and receding contact angles are 90° and 108° respectively.

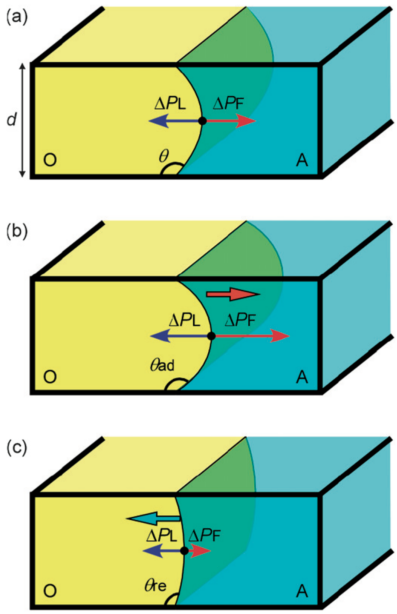

Figure 2.3: A schematic illustration of the balance between the Laplace pressure and the hydrodynamic pressure. (a) The hydrodynamic pressure difference does not exceed the Laplace pressure and a force balance is established. (b) The maximum Laplace pressure is exceeded and the organic phase moves towards the aqueous phase. (c) Here, the minimum Laplace pressure is exceeded and the aqueous phase moves towards the organic phase.[10]

2.3. EXTRACTION LENGTH

The extraction length L_{ext} of the extractor is the length of the main channel, where both phases are in contact. This length must be long enough to ensure a contact time wherein the chemical entity can sufficiently diffuse from the aqueous phase to the organic phase. However, this length is limited by the Laplace pressure, as explained in paragraph 2.2. At the entrance of the extraction channel the pressure difference between the phases is highest. This pressure can not exceed the upper limit of the Laplace pressure ($\Delta p_{lap}(\theta_{ad})$). The maximum extraction length can be derived by equating the expression for the hydrodynamic pressure difference over the length L_{ext} and the Laplace pressure as formulated in equation 2.9 and 2.12 respectively. The expression for the maximum extraction length is formulated in equation 2.14.

$$L_{ext} = \frac{2\gamma \sin(\theta_{contact} - 90°)}{h(Q_{aq}R_{aq} - Q_{org}R_{org})} \tag{2.14}$$

Here, it was assumed that the pressure at the outlet channels is atmospheric, hence $\Delta p_{out} = 0$.

Furthermore, it is of importance that the interface is located in the middle of the channel since the outlet channels have an equal width. Experimental research done by Pohar, Lakner and Plazl, shows a relation between the flow rates and the viscosity's of the phases which ensures the interface to be located in the middle of the channel.[12] The relation is formulated in equation 2.15.

$$\frac{Q_{aq}}{Q_{org}} = (\frac{\mu_{aq}}{\mu_{org}})^{-0.76} \tag{2.15}$$

Combining equation 2.14 and 2.15 gives an expression for the extraction length which ensures clean separation at the end of the channel.

$$L_{ext} = \frac{2\gamma \sin(\theta_{contact} - 90°)}{\frac{\alpha Q_{aq}\mu_{aq}}{w^2 h}(1 - \frac{\mu_{org}}{\mu_{aq}})^{0.24}} \tag{2.16}$$

The analytically obtained result for an optimized extraction length has been reported by Goyal and Desai in 2013[1]. However, in their analysis they used a perimeter expression for a rectangular shaped channel containing only one fluid. Furthermore, due to an algebraic miscalculation they obtained the term $(1 - \frac{\mu_{org}}{\mu_{aq}})^{0.34}$ in the extraction length expression. Using equation 2.16 and 2.7 for the calculations on the extraction length

for the copper extraction as reported in their research, leads to a significant deviation, of about 30%, in the results. For calculations during this research the extraction length will be calculated using equation 2.16.

3

TRANSIENT MASS TRANSFER

Mass transfer is the displacement of mass from one point to another and can be studied at different levels. Individual molecules exhibit Brownian motion, due to their thermal energy. This random walk of molecules has a net displacement in the direction of regions with lower concentrations. This phenomena is called diffusion. Furthermore, mass transfer can be studied at macro scale by looking at the displacement of mass due to the bulk motion. This is called convection. Hence, net mass transfer in a system is often a combination of both diffusion and convection.

This chapter describes the physics behind transient mass transfer in fluids by diffusion. In paragraph 3.1 the basic relations for diffusion are formulated and explained. Paragraph 3.2 describes transient mass transfer, hereby a distinction is made between short- and long time mass transfer. Next, paragraph 3.3 accounts for mass transfer in a two-phase system through a liquid-liquid interface.

3.1. DIFFUSIVE MASS TRANSFER

For a number of cases diffusion can be described by Fick's law. Fick's law gives a relation between the diffusive flux and the concentration under the assumption of steady state. The diffusive flux ϕ''_m is an expression for the flow per unit area, with the area perpendicular to the flow direction. Fick's law can be formulated as equation 3.1.

$$\phi''_m = -D\frac{dc}{dx} \tag{3.1}$$

Here, D is the diffusion coefficient and c the concentration. Equation 3.1 shows that the diffusive flux is always directed towards a region of lower concentration and the flux magnitude is proportional to the concentration gradient. Fick's law only gives a valid description of mass transfer when certain conditions are satisfied. First of all, the system should be binary and consist of a dilute solution. Furthermore, the diffusion molecules should not show high polarity or have non-spherical shapes.[13]

Fick's law can be extended to predict concentration changes over time. This relation is derived by setting up a mass balance for a system containing two different substances. First, the system is in equilibrium, this means that both concentrations are constant. When the concentration of one of the substances is raised, while keeping the total mass in the system constant, the molecules will penetrate the medium. Equation 3.2 shows the mass balance over a thin film from x to $x+dx$.

$$WL\frac{\partial c}{\partial t} = WL(-D\frac{\partial c}{\partial x})_x - WL(-D\frac{\partial c}{\partial x})_{x+dx} \tag{3.2}$$

Here W and L are the width and length of the system in the respectively y and z-direction. The concentration c of the chemical entity varies in the x-direction only, for this simplified system. D represents the diffusion coefficient for the chemical entity. Equation 3.2 can be rewritten to a differential equation.[13]

$$\frac{\partial c}{\partial t} = D\frac{\partial^2 c}{\partial x^2} \tag{3.3}$$

Solving equation 3.3 gives a time- and spatial dependent concentration profile. Figure 3.1 gives a schematic illustration for the diffusion of particles through a medium over time.

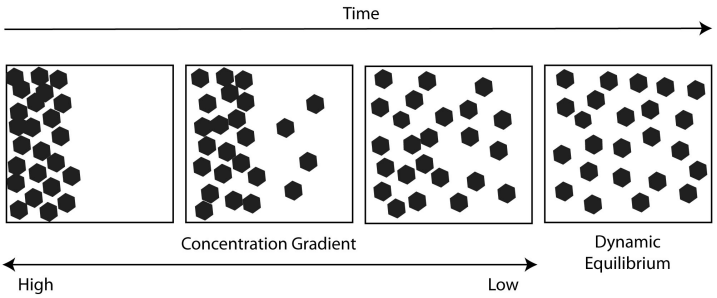

Figure 3.1: A schematic illustration for diffusion of particles in a medium over time. The black dots represent the particles diffusing in the direction of a lower concentration until equilibrium is reached.[14]

Before the differential equation can be solved the right boundary conditions must be formulated. The boundary conditions depend on the system's characteristics. Paragraph 3.2 will give an example for diffusion in a straight forward one-phase system. In paragraph 3.3 a more complex, two-phase, system is discussed.

In fluid dynamics more than one mass transfer phenomena can occur at the same time. As already mentioned, mass transfer can be driven by concentration differences or by convection or both phenomena can occur simultaneously. In many cases it is therefore convenient to make use of dimensionless numbers. These numbers give a ratio for different phenomena. This ratio indicates which of these phenomena is more dominant present and has a higher influence on the system. The dimensionless number of *Péclet* gives the ratio between diffusion time and convection time.[2].

$$Pe = \frac{diffusion_{time}}{convection_{time}} = \frac{\tau^{rad}_{diff}}{\tau^{a}_{conv}} = \frac{\frac{a^2}{D}}{\frac{a}{V}} = \frac{Va}{D} \tag{3.4}$$

Here, a is the radial length over which the concentration changes, V is the velocity of the flow and D is, again, the diffusion coefficient for a chemical entity in a medium. The extraction process that is studied in this research is based on diffusion of the extracting species. Here, it is important that diffusion from one phase to the other has taken place within the contact time of the liquid-liquid interface in the extraction channel. The contact time depends on the flow rates of the fluids. Hence, for sufficient extraction the diffusion time should be lower than the convection time and the system needs to have a small Péclet number.

3.2. PENETRATION THEORY

In paragraph 3.1 Fick's law is introduced. Furthermore, it is explained that a transient mass transfer problem can be solved by equation 3.3 and the right boundary conditions.

The theory of transient mass transfer shows analogies with that of transient heat transfer. When a homogeneous medium is in equilibrium that is, has a constant temperature, and one boundary of the medium is exposed to a higher temperature, the temperature of the medium will gradually change. First, only the temperature of the medium close to the boundary will rise. As time goes by, temperature rise will penetrate through the medium. After long enough time, the medium will reach a temperature equal to the applied temperature. Hence, the heat has penetrated through the complete body and the system has reached equilibrium.

In the case of mass transfer, the flux depends on the mass diffusion coefficient instead of the thermal diffusion coefficient. Furthermore, instead of a temperature change a concentration change is applied in the medium. Consequently, this concentration change will affect the concentration through the medium the same way as a temperature change does.

During the penetration process, two phases can be distinguished. Namely, *short-time penetration* and *long-time penetration*. In the case of short-time penetration, the concentration change is noticeable close to the boundary. Long-time penetration describes the situation where the concentration change has affected the complete medium. Hence the medium is in the process of changing its concentration profile towards a new equilibrium.

The distinction between short-time and long-time penetration is determined by the *penetration length*, this length indicates how far the concentration change has penetrated the medium. Equation 3.2 formulates the expression for the penetration length.

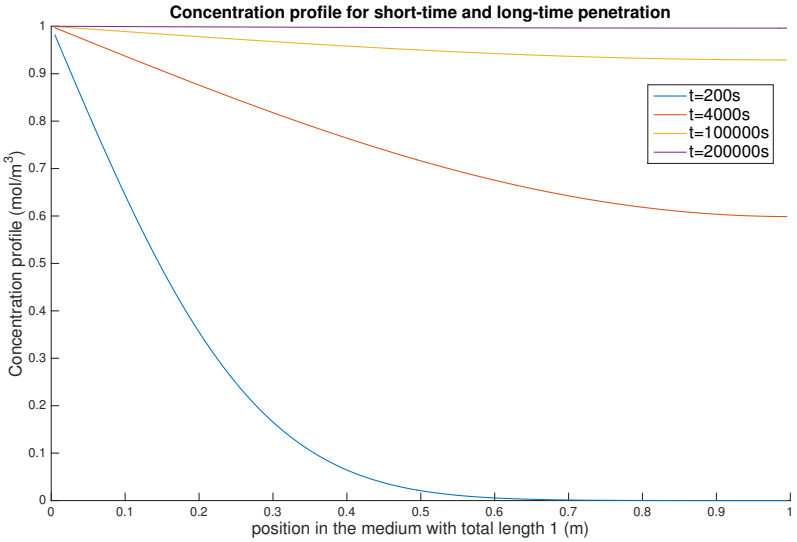

Figure 3.2: The graph shows the concentration profiles at four different moments in time. The *y*-axis represents the concentration level, the *x*-axis represents the position in the medium. The first graph is an example of short-time penetration. The other graphs are examples for long-time penetration. These concentration profiles are based on a diffusion coefficient of $1.17 * 10^{-4} m^2/s$ and a total length of 1 m.

$$L_{penetration} = \sqrt{\pi D t} \tag{3.5}$$

If the penetration length is smaller than 60% of the length over which the diffusion takes place, the system is concerned with short-time penetration. Otherwise, one speaks of long-time penetration. The penetration distinction condition can be reformulated in terms of penetration time using the dimensionless number of *Fourier*. The Fourier number is formulated in equation 3.6.

$$Fo = \frac{Dt}{L^2} \tag{3.6}$$

Here, D is the mass diffusion coefficient, t is the time since the concentration change has been applied. L is the length of the medium along the flux direction. For $Fo < 0.1$ the system is concerned with short-time penetration, when $Fo > 0.1$ the system is exposed to long-time penetration[15].

Figure 3.2 illustrates a concentration profile in a one-phase medium. One-phase, means that the chemical entity is diffusing through one media. The concentration profile is obtained by solving Fick's second law with the following boundary conditions:

$$\begin{aligned} &\text{at } x = 0, \quad c = 1 \\ &\text{at } x = 1, \quad \frac{\partial c}{\partial x} = 0 \end{aligned}$$

Hence, at $x = 0$, the concentration is held at a constant value. As time goes by, the concentration in the rest of the medium is increasing. The first two graphs show examples of short-time penetration, the third graph is an example of long-time penetration in its latest phase, a new equilibrium state is found.

3.3. TWO-PHASE SYSTEM

In the case of a two-phase system interface phenomena make it more complex to solve Fick's law and obtain a concentration profile.

In a two-phase system, assuming both phases to be immiscible, a liquid-liquid interface exists. When a chemical entity is dissolved in phase *A*, it will diffuse through the interface to phase *B*. Figure 3.3 gives an illustration of the concentration profile for this situation. The left picture shows the concentration profile at equilibrium. The right picture shows the concentration profile at a moment in time, while diffusion is taking place and equilibrium is not yet reached.

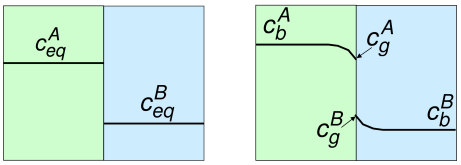

Figure 3.3: Concentration profile for a two-phase system. The left picture shows the concentration profile at equilibrium. The right picture shows the concentration profile at a moment in time. The green layer depicts phase *A*, the blue layer depicts phase *B*. Furthermore, c^A_{eq} and c^B_{eq} denote the equilibrium concentrations in phase *A* and *B* respectively. In the right picture, c^A_b and c^B_b represent the bulk concentrations and c^A_g and c^B_g are the interface concentrations of the chemical entity for both phases[16].

In the case of heat transfer in a two-phase system, equilibrium means that both phases reach the same temperature. However, this is not the case for mass transfer. As can been seen in figure 3.3, when equilibrium is reached, the concentration of the chemical entity is not the same in both phases. This concentration difference is a consequence of the different chemical potential for the solute in both solvents. Equilibrium is attained when the chemical potentials, also known as the partial molal Gibs free energies, are equal in both phases. A partial molal property is a thermodynamic quantity, which indicates how an extensive property of a solution varies when changes occur in the molar composition of the solution. Hence, the free energy in both phases changes during the diffusion process until the chemical potential in both phases is equal. The expression for the chemical potential is formulated in equation 3.7.

$$\mu_i = (\frac{\partial G}{\partial n_i})_{T,P} \tag{3.7}$$

Here, μ_i is the chemical potential for each component of the mixture, G stands for the Gibbs free energy and n_i is the amount of each component of the mixture in moles. For the system as described in figure 3.3, two solvent phases are present and the chemical potential of the solute in each phase must be equal.

$$\mu_1 = \mu_2 \tag{3.8}$$

Equation 3.8 can be rewritten in terms of the solute concentration m (in molality), γ the molal activity coefficient and μ^0, the chemical potential for a hypothetical ideal 1 molal solution.

$$\mu^0_1 + RT\ln m_1 + RT\ln\gamma_1 = \mu^0_2 + RT\ln m_2 + RT\ln\gamma_2 \tag{3.9}$$

Here, R denotes the universal gas constant and T is the temperature. This expression can be rewritten to the ratio of the solute concentrations, which is called the distribution coefficient K_D. The expression for K_D is formulated in equation 3.10.[17]

$$K_D = \frac{m_2}{m_1} = \frac{\gamma_1}{\gamma_2} e^{\frac{-(\mu^0_2 - \mu^0_1)}{RT}} \tag{3.10}$$

Hence, the distribution coefficient is a chemical property which depends on all the substances in the system. K_D can also be denoted by equation 3.11

$$K_D = [\frac{c^B}{c^A}]_{eq} \tag{3.11}$$

Here, c^A and c^B represent the concentration of a solute in respectively solvent *A* and *B*. Hence, K_D gives the ratio of these concentrations as the system is in equilibrium. The gap between the concentration, shown in figure 3.3 in the left picture, is a consequence of the distribution coefficient K_D. This relation is formulated in equation 3.12.[13] For the situation in figure 3.3 K_D is smaller than zero.

$$c^B_{eq} = K_D c^A_{eq} \tag{3.12}$$

The right picture in figure 3.3 shows the concentration profile for a moment in time where the system has not yet reached equilibrium. However, the interface concentrations establish an equilibrium immediately after the solute is added to phase *A*. The interface equilibrium concentrations are related by the same distribution coefficient as specified in equation 3.11. Equation 3.12 can than be rewritten in terms of the interface concentrations, as is formulated in equation 3.13.

$$c_g^B = K_D c_g^A \tag{3.13}$$

In the case of transient processes, as time goes by, the bulk concentration in both phases may change. Consequently, interface concentrations will change over time as well. However, equation 3.13 will always hold.

II

Analysis

4

METHODOLOGY

As stated in part I, the research question for this thesis can be formulated as follows:

What is an accurate simulation model for the extraction process of technetium-99m and what are the optimized parameters for the geometrical design of the microfluidic platform to establish the highest possible extraction efficiency?

In Part I *Literature study*, it is made clear that an efficient extraction depends on the contact time of the phases within the extraction channel. Furthermore, a force balance is needed to establish a clean separation at the end of the extraction channel. Hence, to model the extraction process both diffusion and the pressure balance have to be taken into account.

The two physical phenomena are simulated using MATLAB. By varying the geometrical parameters of the extraction channel, the influence on the extraction length (L_{ext}) is determined. Furthermore, the diffusion process of technetium-99m from the aqueous phase to 2-butanone is simulated by a numerical model. Hereby, the concentration profile at a moment in time can be simulated while varying the width of the extraction channel. Eventually, a numerical optimization is conducted to obtain optimized parameter combinations that result in a high extraction efficiency.

Furthermore, it is of great importance that a two-phase immiscible flow is established in the channel. The flow of the aqueous phase and 2-butanone are studied by an experiment.

In this chapter the methods applied for the analysis on the extraction process are described. Paragraph 4.1 describes the numerical model that is used for the calculations on the force balance and on the diffusion model. In paragraph 4.2 the experimental set-up is described.

4.1. NUMERICAL SIMULATION

In this paragraph the calculations on the force balance and are treated and a diffusion model for pertechnetate is presented.

4.1.1. CALCULATIONS ON THE FORCE BALANCE

In chapter 2 is explained which condition must hold to obtain clean separation. The condition is given by equation 2.1. From this relation an expression for the extraction length L_{ext} was derived as formulated in equation 4.1.

$$L_{ext} = \frac{2\gamma \sin(\theta_{contact} - 90^\circ)}{\frac{\alpha Q_{aq} \mu_{aq}}{w^2 h}(1 - \frac{\mu_{org}}{\mu_{aq}})^{0.24}} \tag{4.1}$$

The optimized extraction length depends on the chemical properties of the substances, the geometrical parameters of the channel and on the flow rate of the phases. The chemical properties that are relevant for the extraction of technetium-99m using an aqueous solution and 2-butanone, are listed in table 4.1. Most values were found in literature [17][11]. The diffusion coefficient for pertechnetate in 2-butanone is approximated by equation 4.2[18].

water	
viscosity	0.890 mPas
surface tension	72.8 mN/m
solubility MEK	12.5%
2-butanone (MEK)	
viscosity	0.405 mPas
surface tension	24.6 mN/m
solubility in water	26.8 %
pertechnetate ($99TcO_4^-$)	
diffusion coefficient in water	$1.48*10^-9$ m^2/s
diffusion coefficient in MEK	$1.09*10^-9$ m^2/s
concentration $99TcO_4^-$	10^-6 mol/m^3
PDMS	
hydrophobicity	highly hydrophobic
contact angle with water	108°
other	
interfacial tension water and MEK	48.2 mN/m
distribution coefficient water/MEK	778

Table 4.1: Overview of the chemical properties of the substances present in the extractor. These values are used for the calculations of the extraction length L_{ext}.[17][11]

parameter	*range*	*conditions*
width (w)	10-100μm	height = 50 μm and flow rate = 20 μm
flow rate (Q_{aq})	10-100μL/min	height = 50 μm and width = 100 μm
height (h)	10-100μm	flow rate = 20 μm and width = 100 μm

Table 4.2: Overview of parameter variations for the calculations of the extraction length L_{ext}.

$$D_{AB} = \frac{k_B T}{6\pi\mu_B\sigma_A} \tag{4.2}$$

Here, k_B is the Boltzmann constant, μ_B the viscosity of liquid B and σ_A is the diameter of the diffusing molecule. As contact angle the value applicable to PDMS in combination with water is used as an approximation for the contact angle of water with 2-butanone and PDMS. Finally, a distribution coefficient for a aqueous solution with pertechnetate and pyridine is used, instead of 2-butanone. The approximations are a consequence of too little information available in literature. These variables can be determined more accurately by future experimental research.

The other parameters can be varied to test the influence on the extraction length. The variations that are performed for the calculations are listed in table 4.2. The *conditions* in table 4.2 are the parameters set constant while varying the other parameter.
The values chosen for the conditions are based on results by Goyal and Desai.[1] In their paper they reported good extraction results for w=100 μm, Q_{aq}=20 μL/min h=50 μm for the extraction of copper. Here, w is the half-width of the channel, thus the width for one phase as the interface is located in the middle of the channel.

The calculations are conducted as follows: First, the extraction length is calculated for each parameter individually. Finally, the relation for the extraction length and all three variables is calculated. In chapter 5 the results for the calculations are presented.

4.1.2. DIFFUSION MODEL

As is described in chapter 3, diffusion can be analyzed using Fick's law. For the flow in the extractor we assume plug flow and Fick's law can be used to model the diffusion of the technetium compounds from the aqueous phase to the organic phase. The differential equation 4.3 is solved numerically in MATLAB for each phase.

$$\frac{\partial c_i}{\partial t} = D_i \frac{\partial^2 c_i}{\partial x^2} \tag{4.3}$$

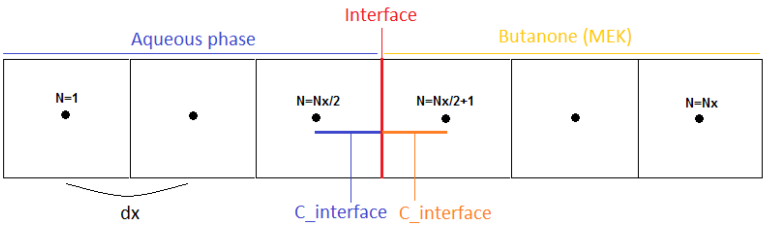

Figure 4.1: An illustration of the grid design used to simulate the diffusion process. Made by A.Blok

Both sides of equation 4.3 can be discretized. Figure 4.1 shows the one-dimensional grid over which the discretization is done. Equation 4.4 and 4.5 formulate the discretized expressions.

$$\frac{\partial c_i}{\partial t} \rightarrow \frac{c_N^{i+1} - c_N^i}{\Delta t} \tag{4.4}$$

$$D_i \frac{\partial^2 c_i}{\partial x^2} \rightarrow D(-\frac{c_N - c_{N-1}}{\Delta x} - (-\frac{c_{N+1} - c_N}{\Delta x})) \rightarrow \frac{D}{\Delta x^2}(c_{N-1} + c_{N+1} - 2c_N) \tag{4.5}$$

Combining equation 4.4 and 4.5 results in the discrete differential equation 4.6, which must be solved, to obtain the concentration profile for the technetium compounds.

$$\frac{c_N^{i+1} - c_N^i}{\Delta t} = \frac{D}{\Delta x^2}(c_{N-1}^i + c_{N+1}^i - 2c_N^i) \tag{4.6}$$

Here, $i+1$ and $N+1$ or $N-1$ represent the time steps and spatial displacement respectively. Rewriting equation 4.6 gives an expression for the concentration profile depending on time and position as is shown in equation 4.7.

$$c_N^{i+1} = \frac{D\Delta t}{\Delta x^2}(c_{N-1}^i + c_{N+1}^i) + c_N^i(1 - 2\frac{D\Delta t}{\Delta x^2}) \tag{4.7}$$

To obtain a concentration profile for the extraction of technetium compounds, boundary conditions and initial conditions, that specify the extraction system, have to be taken into account. As is mentioned in chapter 3, at the interface an equilibrium is established immediately. This equilibrium depends on the bulk concentrations of techentium-99m in the aqueous and organic phase and is related by the distribution coefficient K_D. The interface concentrations are expressed as a boundary conditions. They can be derived using equation 4.8. Equation 4.8 states that the mass flux through the left side of the interface is equal to the mass flux through the right side of the interface.

$$-D_w \frac{dc}{dx}|_{left} = -D_b \frac{dc}{dx}|_{right} = \phi_m'' \tag{4.8}$$

Discretizing this equation results in expression 4.9.

$$-D_w(\frac{c_{int}^w - c_{Nx/2-1}}{1\frac{1}{2}\Delta x}) = -D_b(\frac{c_{Nx/2+2} - c_{int}^b}{1\frac{1}{2}\Delta x}) \tag{4.9}$$

Here, c_{int}^w and c_{int}^b denote the interface concentrations in the aqueous solution and 2-butanone respectively. Together with the relation for the equilibrium concentrations at the interface and K_D.

$$c_{int}^b = K_D c_{int}^w \tag{4.10}$$

The concentrations at the interface can be expressed by equation 4.11 and 4.12.

$$c_{int}^w = c_{N_x/2}^{i+1} = \frac{D_b c_{N_x/2+2}^{i+1} + D_w c_{N_x/2}^{i+1}}{D_b K_b + D_w} \tag{4.11}$$

boundary conditions	*formula*
no flux through the left boundary	$c_1^{i+1} = c_1^i(1 - \frac{D\Delta t}{\Delta x^2}) + c_2^i \frac{D\Delta t}{\Delta x^2}$
no flux through the right boundary	$c_{N_x}^{i+1} = c_{N_x}^i(1 - \frac{D\Delta t}{\Delta x^2}) + c_{N_x-1}^i \frac{D\Delta t}{\Delta x^2}$
interface equilibrium in aqueous phase	$c_{int}^w = c_{N_x/2}^{i+1} = \frac{D_b c_{N_x/2+2}^{i+1} + D_w c_{N_x/2}^{i+1}}{D_b K_b + D_w}$
interface equilibrium in organic phase	$c_{int}^b = c_{N_x/2+1}^{i+1} = \frac{D_b c_{N_x/2+2}^{i+1} + D_w c_{N_x/2}^{i+1}}{D_b + \frac{D_w}{K_D}}$
initial conditions	*expression*
the concentration Tc-99m in aqueous phase at $t = 0$	$c_{aq}^1 = 10^{-6}$ mol/m^3
the concentration Tc-99m in the organic phase at $t = 0$	$c_{org}^1 = 0$ mol/m^3

Table 4.3: Overview of the boundary and initial conditions for the extraction of technetium-99m. These conditions are used for solving equation 4.7.

$$c_{int}^b = c_{N_x/2+1}^{i+1} = \frac{D_b c_{N_x/2+2}^{i+1} + D_w c_{N_x/2}^{i+1}}{D_b + \frac{D_w}{K_D}} \tag{4.12}$$

The no-flux conditions, applied to the boundaries of the grid shown in figure 4.1, are derived using equation 4.7. To derive the no-flux condition at the left boundary of the grid, c_{N-1}^i is taken to be zero. This results in the expression.

$$c_1^{i+1} = c_1^i(1 - \frac{D\Delta t}{\Delta x^2}) + c_2^i \frac{D\Delta t}{\Delta x^2} \tag{4.13}$$

For the derivation of the no-flux condition at the right boundary of the grid, c_{Nx+1}^i is taken to be zero. The right boundary condition is formulated in equation 4.14.

$$c_{N_x}^{i+1} = c_{N_x}^i(1 - \frac{D\Delta t}{\Delta x^2}) + c_{N_x-1}^i \frac{D\Delta t}{\Delta x^2} \tag{4.14}$$

The boundary conditions and initial conditions are summarized in table 4.3.
Here, $N_x = \frac{2w}{\Delta x}$ is the maximum number of steps over the total width of the channel (w is the half-width of the channel). For $N = [1, \frac{N_x}{2}]$, $D = D_w$, the diffusion coefficient in water. For $N = [\frac{N_x}{2} + 1, N_x]$, $D = D_b$, the diffusion coefficient in 2-butanone.

With the boundary conditions set, the diffusion process can be simulated. The MATLAB code can be find in Appendix A. The chemical properties used in the simulation are presented in table 4.1. The results of the simulation are presented in chapter 5. The calculations on the force balance and the diffusion profile are combined in the optimization that is conducted to find the geometrical parameters that ensure a maximal efficiency. The results for the optimization are presented in paragraph 5.1.3 and the MATLAB code is attached in Appendix B.

4.2. EXPERIMENTAL SIMULATION

Since it is of great importance that a two-phase immiscible flow is established in the channel, the flow for the aqueous phase and organic phase are studied by an experiment. The solubility of 2-butanone in water

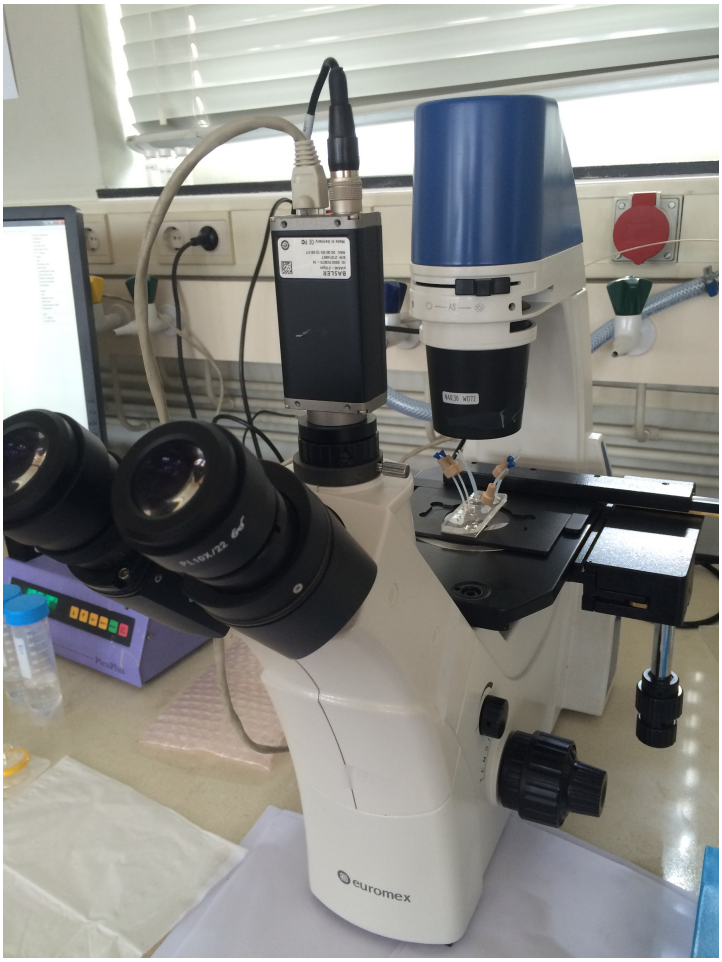

Figure 4.2: A picture of the experimental set-up. The microscope is shown together with the chip. Here, the chip is not yet connected to the pump, the connection is made with the tubing glued on the chip.

and visa verse is presented in table 4.1. The solubility's are quite high, consequently one would expect the solutions to mix. However, when a pure water solution is replaced by a molybdenum solution the solubility decreases significantly and an immiscible flow is expected. This experiment determines whether an immiscible flow is obtained for the combination of molybdenum solution and 2-butanone.

4.2.1. EXPERIMENTAL SET-UP

As mentioned in the previous chapters, the aqueous solution exists of a molybdenum solution and for the organic solution 2-butanone was used. To obtain the molybdenum solution, 6.5 g of $(NH_4)_6Mo_7O_{24}\bullet 4H_2O$ was dissolved in 17.2 ml of H_2O and 1 ml of H_2O_2. The chip that was used for the experiment is made of PDMS. The half-width of the channel is 100μm, the channel height was 63μm and the channel length was 2 mm. The angle between the inlet and outlet channels was 53°. The chip was designed before this study started and the dimensions are based on previous research.[1]

The two inlet channels were connected to a pump, The two outlet channels were open and therefor exposed to atmospheric pressure. The chip was studied with a Zeiss Primovert microscope with a magnification of 400. The flow pattern was recorded by a camera from Basler and the data was directly send to the computer. Hence, the flow could be monitored live on the computer. In figure 4.2 a picture is shown of the experimental set-up. The experiment was conducted with flow rates of 2 μL/min, 5μL/min, 10μL/min, 20μL/min and 30μL/min Furthermore, the experiment was repeated with a pure water solution instead of the molybdenum solution. From this we were able to see the difference in behavior of the flow when the solubility of the solutions in each other is higher. The results of the experiment are presented in chapter 5

5

RESULTS

This chapter presents the results of this research. The results for the numerical simulations are presented in paragraph 5.1. The results for the experiment are presented in paragraph 5.2.

5.1. NUMERICAL RESULTS

During the numerical simulations, force balance calculations were performed. Furthermore the diffusion process was simulated while varying the width of the channel. Finally, an optimization is conducted on all the geometrical parameters and the flow rate to establish an optimal extraction efficiency. The results are presented in this paragraph.

5.1.1. FORCE BALANCE

To determine the maximum extraction length, the difference in hydrodynamic pressure is plotted versus the maximum Laplace pressure for θ_{ad}. An example of this plot is shown in figure 5.1.

The intersection of the graphs is at the maximum extraction length (L_{ext}=16.5 mm). The graph is plotted for Q_w=20μL/min, h=50 μm, w=100 μm and θ_{ad}=108°. Obviously, varying the parameters will result in different extraction lengths. As proposed in table 4.2, for each parameter the influence on the extraction length is studied. The results are shown in figure 5.2 on page 29. In the first plot the relation between the extraction length and the width is shown, the second graph shows the relation between the extraction length and the flow rate and finally the last plot shows the relation between the extraction length and the height of the channel.

From the graphs it can be concluded that a larger width and height results in a longer extraction length. This can be explained by the hydrodynamic pressure difference. For the hydrodynamic pressure difference and the height and the width, the following relation applies $\Delta p_{hyd} \sim \frac{(2w+h)^2}{(wh)^3}$. For a combination of large height and width the hydrodynamic pressure difference is small. When the hydrodynamic pressure difference is small a longer extraction length is allowed without exceeding the Laplace pressure. Furthermore, the extraction length is longer for lower flow rates. This is a logic consequence of the expression for the extraction length $L_{ext} \sim \frac{1}{Q_{aq}}$. Also, it can been seen that the hydrodynamic pressure difference decreases for lower flow rates. By the same reasoning as with the large width and height, this will result in a longer extraction length. The change in the extraction length is largest for the variation of channel height, here the extraction length range is [0,5 mm,88.1 mm]. From this it can be expected that small variations in channel height have more influence on the extraction length than variations in the other two parameters. The relation between the extraction length, channel width and flow rate, is plotted in figure 5.3 on page 30 for two different values of the height. The first graph is plotted for a channel height of 50 μm and in the second plot the channel height is set at 100 μm. In each plot the different lines represent the flow rates. The flow rate increases from left to right from 10 μL/min to 100μL/min. As expected from the plots in figure 5.2 the extraction length is the longest for low flow rates and large channel heights and widths. A longer extraction length corresponds to a longer contact time of the phases. Whether an extraction length as long as possible is necessary, depends on the diffusion rate of the technetium from the aqueous phase to 2-butanone.

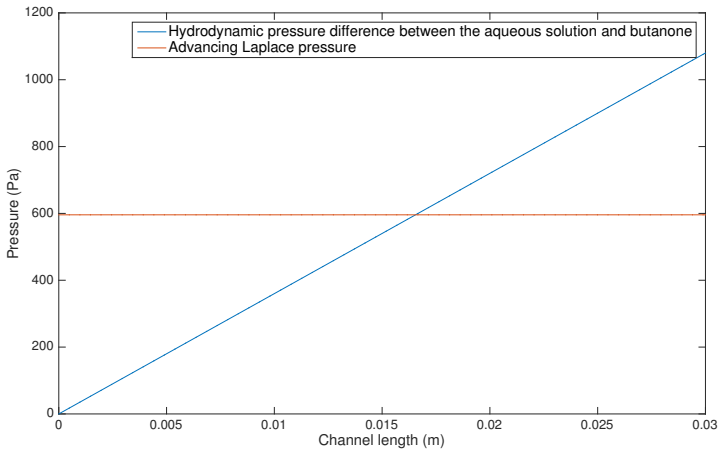

Figure 5.1: The hydrodynamic pressure difference between the phases plotted in blue versus the length of the channel. In red the Laplace pressure is plotted for the advancing contact angle of 108°. The receding contact angle is 90°, here the Laplace pressure is zero. The graphs are plotted for Q_w=20μL/min, h=50 μm and w=100 μm.

5.1.2. DIFFUSION MODEL

The goal of the simulation of the diffusion process is to be able to calculate how much of the pertechnetate is extracted whitin the contact time. Consequently, the extraction efficiency can be calculated for different geometrical parameters.

The diffusion process depends on the chemical properties of pertechnetate, the aqueous solution and 2-butanone. Furthermore, the width of the channel determines the diffusion length. Hence, this is a parameter which can be varied. Figure 5.4 on page 31 shows the concentration profile for pertechnetate in a aqueous solution and in 2-butanone. The plots are taken at different moments in time. Clearly, a shift of the concentration, from one phase to the other, is shown over time. At t=0.1s the curve at the interface is steep and the gradient high. However, as time goes by the gradient decreases and the mass flux through the interface decreases as well. Table 5.1 presents the gradients and mass fluxes for the three moments in time, as shown in the graphs in figure 5.4. The mass flux is calculated using equation 3.1.

time	*position in channel (L)*	*gradient in aqueous phase*	*mass flux through the interface* (ϕ''_m)
t=0.1s	6.67 mm	-4.567$*10^-$8 mol/m^4	6.759$*10^-$17 mol/sm^2
t=1s	6,67 cm	-1.458$*10^-$8 mol/m^4	2.159$*10^-$17 mol/sm^2
t=7s	46.62 cm	-1.518$*10^-$9 mol/m^4	2.246$*10^-$18 mol/sm^2

Table 5.1: The gradient and mass flux through the interface for pertechnetate at t=0.1s, t=1s and t=7s.

Between 0.1 s and 1 s the mass flux has decreased 68%. Between 0.1 s and 7 s the mass flux has decreased almost 97%. This indicates that the diffusion rate decreases much faster at the beginning of the process. Hence, the amount of extracted species is not linearly with time. To obtain a high extraction efficiency, the contact time should at least be long enough to include the highest mass fluxes. Furthermore, variations of the channel width has influence on the amount of pertechnetate extracted. When the channel width is smaller, the volume of the channel is smaller and less pertechenate is present in the channel compared to a channel with a larger width. However, the extraction length, and hereby the contact time, is a limiting factor on the extraction process. When the channel width is chosen smaller, less contact time is needed to extract the present pertechnetate from the molybdenum solution. The difference in efficiency between a channel width of 50 μm and of 100 μm is shown in table 5.2. From the table it can be concluded that, even with a

channel half-width	*time (t)*	*extraction efficiency (%)*	*amount extracted pertechnetate (mol/m^2)*
50 μm	t=1s	81%	4.01$*10^-$11 mol/m^2
100 μm	t=1s	44 %	4.34$*10^-$11 mol/m^2

Table 5.2: The amount of pertechnetate extracted for different channel half-width.

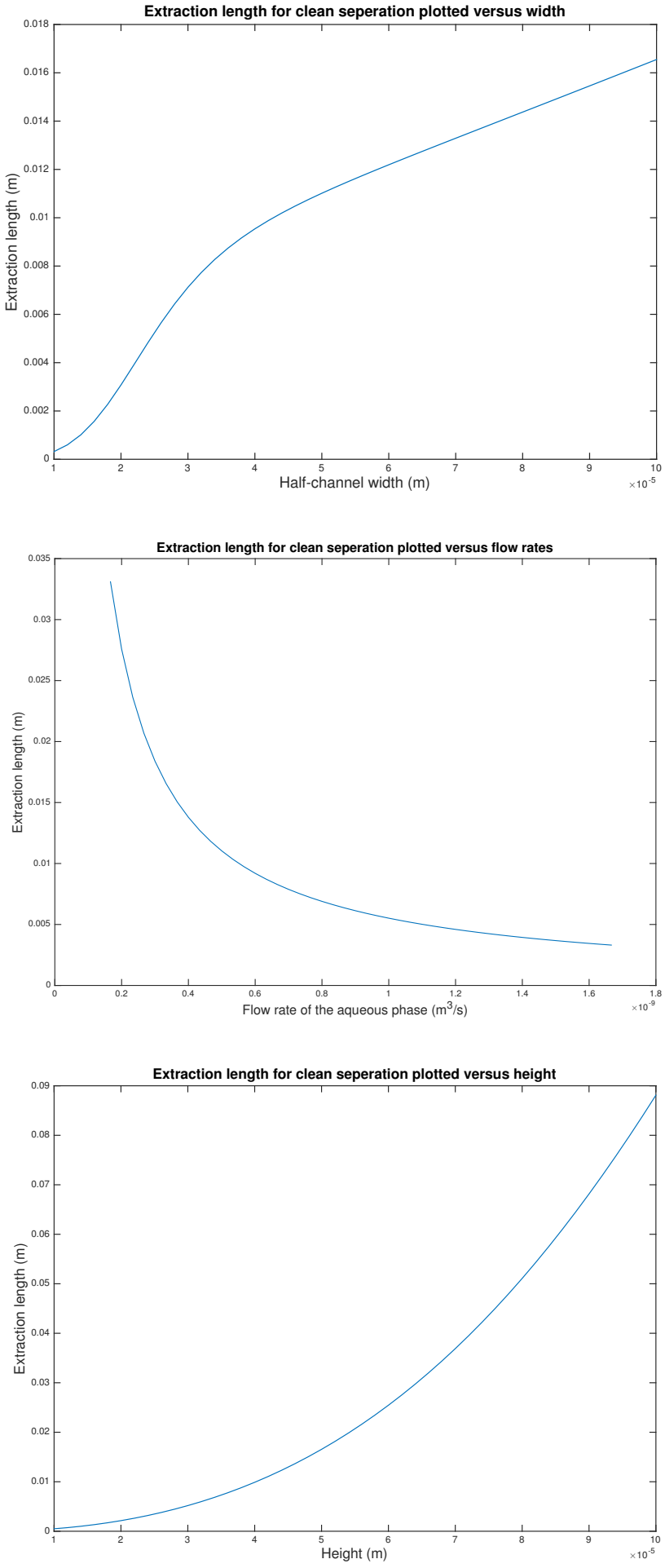

Figure 5.2: The plots show the relation between the extraction length and the width, flow rate and height respectively. The parameters that were kept constant are given in table 4.2

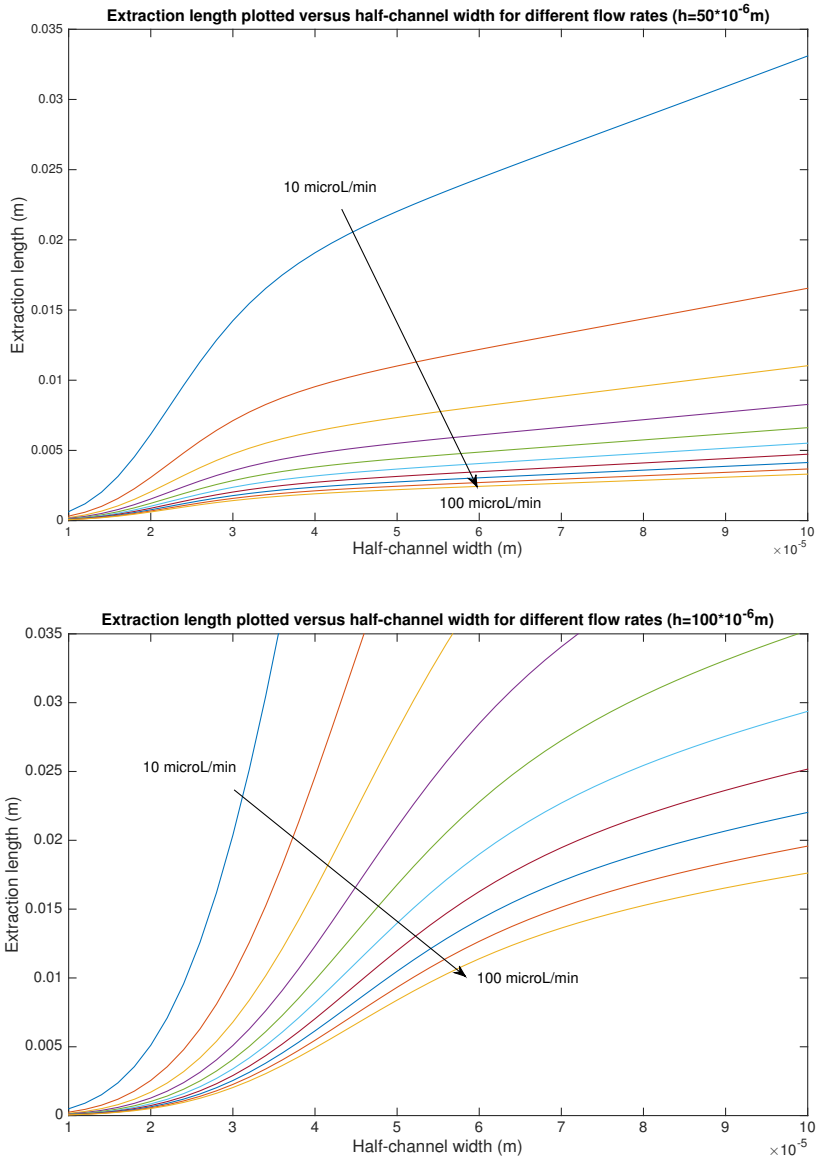

Figure 5.3: The extraction length plotted versus the channel width for different flow rates. In the first plot the channel height is set at 50μm, in the second plot the height is set at 100μm. In both plots the flow rate increases from left to right from 10 μL/min to 100μL/min.

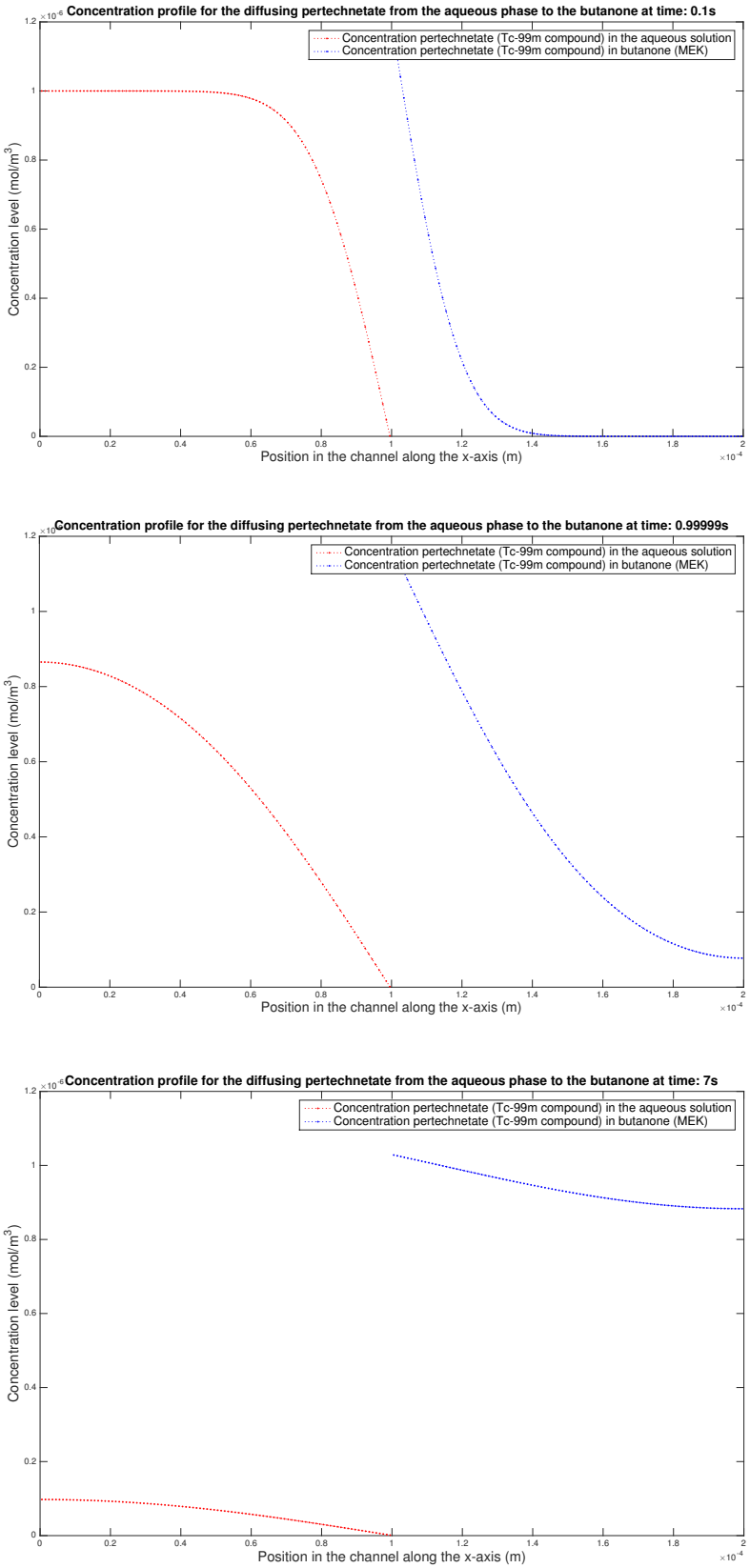

Figure 5.4: Concentration profiles at different moments in time for the diffusion of pertechnetate. The plots are at t=0.1 s t=1 s and t=7 s respectively. The half-width of the channel is set at 100μm.

lower extraction efficiency, the total amount of pertechentate extracted is higher. However, when the total contact time between the phases is 1s, the channel design with a width of 50 μm has extracted 81% of the present pertechnetate from the molybdenum solution. For this design the remaining pertechnetate in the molybdenum solution is significantly lower compared to the channel with an efficiency of 44%. In paragraph 5.1.3 an optimization is conducted for the geometrical parameters and flow rates. Hereby, the extraction efficiency is optimized. This way the resulting design parameters can be used to create an extractor with a maximal extraction efficiency. Hence, this extractor will leave only a low amount of pertechnetate behind in the waste-product. The extractor can than be integrated in a continuous process with a continuous supply of pertechnetate in the molybdenum solution.

5.1.3. OPTIMIZATION

In paragraph 5.1 and 5.1.2 the results are presented for the calculations on the pressure balance and the concentration profile. Now, it is interesting to connect these results and find the optimized geometrical parameters for an efficient extractor. First the optimal extraction length is calculated for Q_{aq} in the range [10μL/min,100μL/min], w in the range [10μm,100μm] and h in the range [10μm,100μm]. Next, the contact time is derived from the optimal extraction length and flow rate. The contact time and width are used to calculate the amount of diffused pertechentate through the interface. The extraction efficiency is calculated by equation 5.1.

$$Efficiency = \frac{\int_w^{2w} c(x)dx}{c_0(1-\frac{1}{1+K_d})w} * 100\% \tag{5.1}$$

For the optimization four test cases are proposed:

1. To obtain the highest extraction efficiency possible, what are the corresponding geometrical parameters and flow rate?

2. If the extraction length is limited by the chips dimensions, take $L_{ext} < 0.01m$. What is the extraction maximal efficiency that can be reached?

3. As described in paragraph 5.2 bubble formation and break-ups in the flow ware observed at flow rates lower than 20 μL/min. To overcome potential bubble formation or slug flow a high flow rate is preferred. What extraction efficiency can be reached if the lower limit on the flow rate range is increased to 20μL/min? Hereby, the condition proposed in test case 2 is still applied.

4. Since previous research shows extraction efficiency's above 90% for a channel height of 50μm [1], it is interesting to compare the efficiency that can be reached when our system is limited to a channel height of 50μm. Test case 4 repeats the optimization with all conditions proposed in the previous test cases including a limitation on the height.

For the first test case the extraction efficiency is taken as parameter which must be maximized. All the ranges, for the geometrical parameters and flow rate, are tested. The result is presented in table 5.3

parameters	
half-width	61.43μm
height	100.00μm
flow rate	$1.67*10^{-10}$ m^3/s
result	
extraction length	0.12 m
extraction time	4.33 s
extraction efficiency	99 %

Table 5.3: Results for test case 1. Optimization of the extraction efficiency.

The results show, that this parameter combination leads to a relative long extraction length and enough contact time to extract almost all pertechnetate from the aqueous phase to the 2-butanone. In Figure 5.5 the optimum of 99% efficiency is plotted. Furthermore, the parameter combinations that lead to extraction efficiencies of 90%, 70% and 40% are shown in the figure. The figure shows clear layers with an optimum for the

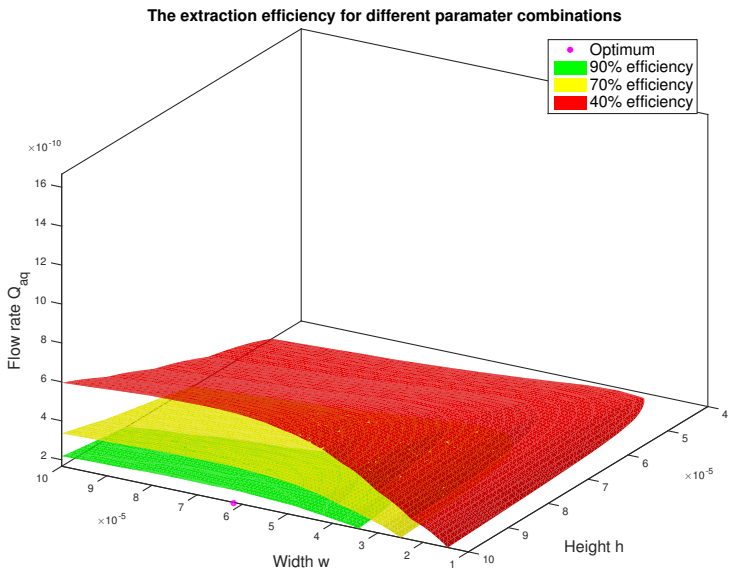

Figure 5.5: Results for test case 1: The graph shows the optimum of 99% efficiency. Furthermore, the extraction efficiencies of 90%, 70% and 40% are shown for the associated parameter combinations

lowest possible flow rate, largest possible height and a channel width of 61.43μm, as is presented in table 5.3. Lower efficiencies are obtained for higher flow rates and smaller heights. The efficiencies plotted in figure 5.5 are meant as an example and illustration of the parameter combinations that lead to lower efficiencies.

The extraction efficiency of 99% is a desired result. However, a channel length shorter than 0.12 m is preferred, since the dimensions of a chip are smaller. For the second test case, the optimization is done including a limiting condition on the extraction length. Namely: L_{ext} can not be larger than 0.01m. The results of the simulation are presented in table 5.4. The table shows that the limitation on the extraction

parameters	
half-width	22.86 μm
height	100 μm
flow rate	$1.67*10^{-10}$ m^3/s
result	
extraction length	8.09 mm
extraction time	0.11 s
extraction efficiency	64 %

Table 5.4: Results for test case 2. Optimization of the extraction efficiency with a limited extraction length (L_{ext}<0.01m)

length lowers the maximum extraction efficiency to 64%. The flow rate and height are not changed compared to the results in table 5.3. The extraction length is 8.09 mm which is a length that can be integrated on a microchip. Figure 5.6 shows the optimum of 64% and the efficiencies of 60%, 40% and 30%. The best results are found for relatively small widths. The flow rate is low and the height has relatively high values.

It is a logical consequence that low flow rates result in a high efficiency. Since a low flow rate maximizes the contact time between the phases. The experiment, described in chapter 4.2.1, shows a most stable flow without bubble formation and slug flow, for a flow rate of 20μL/min. In the third test case the lower limit of the flow rate range is adjusted to 20μL/min. The results for the third test case are presented in table 5.5.

Table 5.5 shows, again, a decrease in extraction efficiency. This result could be expected since the flow rate is increased. The extraction length is almost 1 cm and the channel width has increased a little compared to the result of test case 2. Figure 5.7 shows the optimum of 44% and the efficiencies of 40%, 35% and 30%. Again, the best results are found for relatively small widths ans larges heights. The flow rate is equal to the new lower limit of $3.33*10^{-10}$ m^3/s.

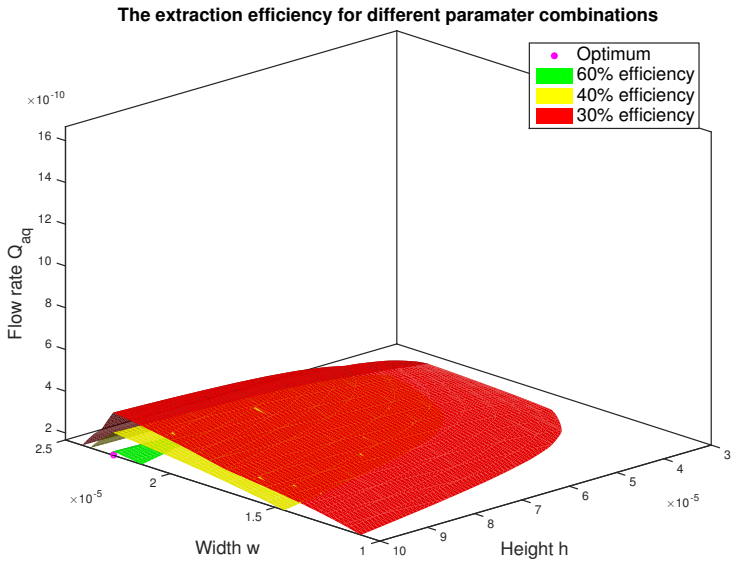

Figure 5.6: Results for test case 2: The graph shows the optimum of 64% efficiency. Furthermore, the extraction efficiencies of 60%, 40% and 30% are shown for the associated parameter combinations. Here, the condition of a limited extraction length is applied.

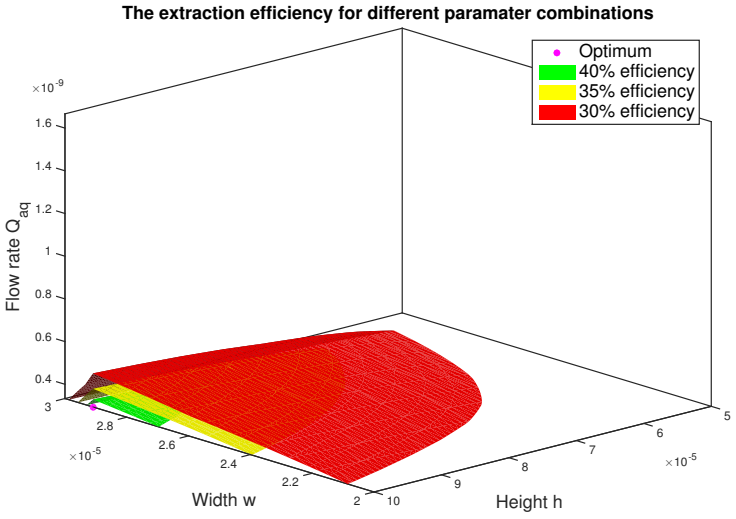

Figure 5.7: Results for test case 3: The graph shows the optimum of 44% efficiency. Furthermore, the extraction efficiencies of 40%, 35% and 30% are shown for the associated parameter combinations. Here, the condition of a limited extraction length is applied and the lower limit of the flow rate is adjusted to 20μL/min

parameters	
half-width	29.29 μm
height	100 μm
flow rate	$3.33*10^{-10}$ m^3/s
result	
extraction length	9.41 mm
extraction time	0.08 s
extraction efficiency	44 %

Table 5.5: Results for test case 3. Optimization of the extraction efficiency with a limited extraction length (L_{ext}<0.01m) and a flow rate range of [20 μL/min, 100μL/min]

In the last test case the height range is adjusted. The upper limit is decreased to 50 μm. Since, so far, the best results corresponds to the highest possible height, it can be expected that the extraction efficiency will decrease significantly when the height has a lower upper limit. The results for the fourth test case are presented in table 5.6.

parameters	
half-width	35.71 μm
height	50 μm
flow rate	$3.33*10^{-10}$ m^3/s
result	
extraction length	8.68 mm
extraction time	0.05 s
extraction efficiency	27 %

Table 5.6: Results for test case 4. Optimization of the extraction efficiency with a limited extraction length (L_{ext}<0.01m), a flow rate range of [20 μL/min, 100μL/min] and a height range of [10μm, 50μm]

Figure 5.8 on page 37 shows the optimum of 27% and the efficiencies of 10%, 8% and 5%.

5.2. EXPERIMENTAL RESULTS

The experiment conducted with a molybdenum solution and 2-butanone showed bad results for flow rates lower than 10μL/min. The best result was obtained at 20μL/min. In some flow profiles bubble formation was observed. This can be a consequence of bubble formation during the solution preparation. Since, solutions contain air, normally this the solutions are degassed by putting vacuum on them while they are in an ultrasonic bath, this is not done for our experiment. However, most bubbles were observed at low flow rates, thus the bubble formation might be initiated as well for too low flow rates. For each flow rate tested a picture of the flow profile is presented in figure 5.9 on page 38. The pictures show, from top to bottom, the flow profile for the flow rates 2 μL/min, 5μL/min, 10μL/min, 20μL/min and 30μL/min respectively. The molybdenum solution comes in from the top right inlet and 2-butanone comes in from the right inlet at the bottom.

The first picture, at 2 μL/min, shows that the 2-butanone is suppressed by the molybdenum solution. As explained in subparagraph 5.1, for low flow rates is takes a longer time to reduce the contact angle from 108° to 90°. In this picture it seems that the Laplace pressure exceeds the hydrodynamic pressure difference and the interface is shifted to the side. In the second picture, bubble formation is shown. Here the flow rate was set at 5μL/min. It is not clear whether the bubbles are already present in the solution before entering the channel or if the bubbles are a consequence of the low flow rate. For future experiments, it should be made sure that the bubble formation in the solution is minimized. The third picture is made for a flow rate of 10μL/min. The flow is more stabilized than in the previous pictures. However, the interface is shifting as the flow evolves. This results in a leakage of 2-butanone in the molybdenum solution. The fourth picture, shows the best result of the experiment. Here the flow rate is set at 20 μL/min. The interface is stable during the flow and is more or less located in the middle of the channel. Unfortunately, when the flow reaches the outlet channels, the separation is not clean. Leakage of the 2-butanone in the molybdenum solution is observed. The fifth picture, for 30μL/min, shows bubble formation. Here the bubbles were sticking to the wall for a while and hereby they pushed the molybdenum solution in the direction of the 2-butanone. Consequently, the interface was less stable than for a flow rate of 20 μL/min. Here, as well leakage is observed from 2-

butanone into the molybdenum solution.

From a practical point of view, leakage of 2-butanone to the molybdenum solution is less problematic than the other way around. The 2-butanone has to remain pure, without other products from the molybdenum solution. When 2-butanone leaks into the molybdenum solution only the extraction efficiency decreases but the remaining 2-butanone with pertechnetate is still usable.

The leakage of 2-butanone into the molybdenum solution can be a consequence of the hydrophobic channel walls. The molybdenum solution feels a repulsive force from the wall and therefor gives room to 2-butanone, which does not feel any repulsive forces from the wall, to enter the upper outlet channel.

As mentioned in chapter 4, the experiment is repeated with the molybdenum solution replaced by a pure water solution. Figure 5.10 on page 39 shows the results of the experiment for flow rates of 1 μL/min, 5μL/min and 12μL/min. From the pictures is can be concluded that for all flow rates the interface is not stable or located in the middle. The pictures are only snapshots but the movies show constantly break-ups of the aqueous phase. This can be a consequence of the relatively high solubility of 2-butanone in water.

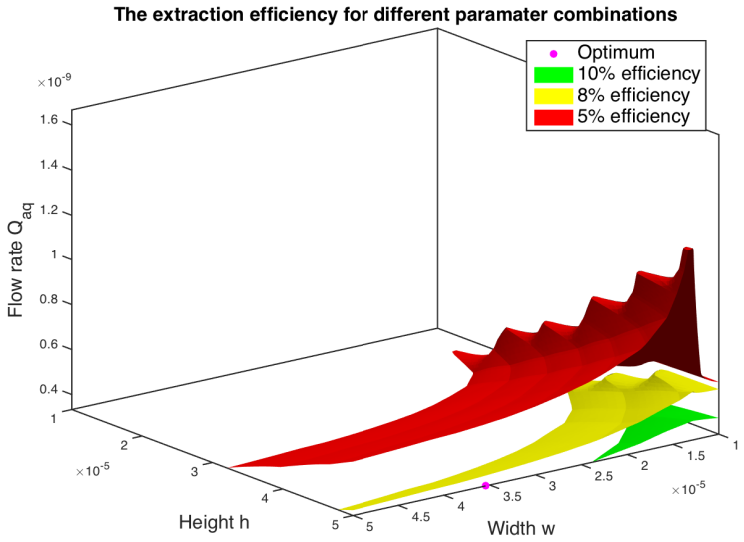

Figure 5.8: Results for test case 4: The graph shows the optimum of 27% efficiency. Furthermore, the extraction efficiencies of 10%, 8% and 5% are shown for the associated parameter combinations. Here, the condition of a limited extraction length is applied, the lower limit of the flow rate is adjusted to 20μL/min and the upper limit for the height is adjusted to 50μm.

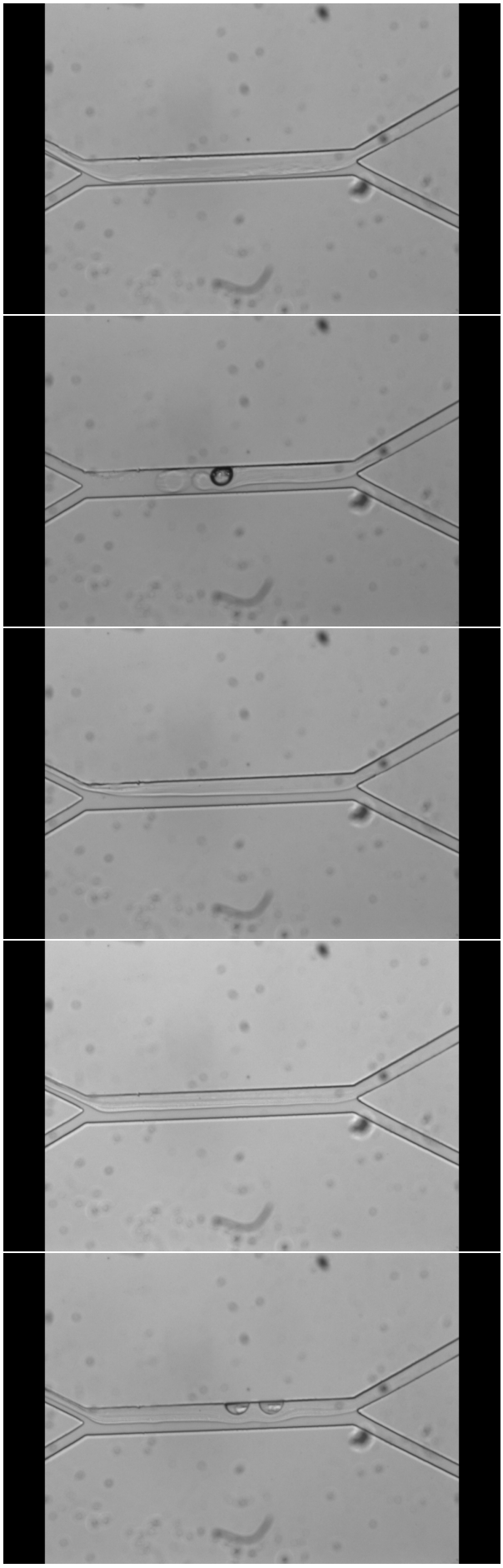

Figure 5.9: Pictures of the flow profile for flow rates of 2 μL/min, 5μL/min, 10μL/min, 20μL/min and 30μL/min from the top to bottom respectively.The flow is from right to left. The molybdenum solution comes in from the top inlet and 2-butanone from the bottom inlet.

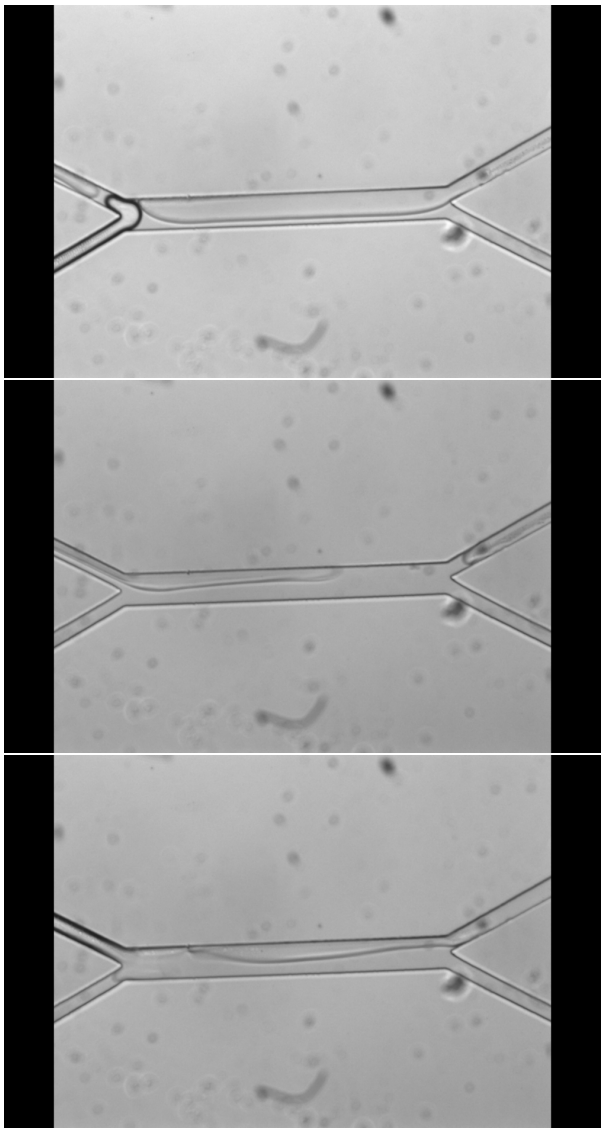

Figure 5.10: Pictures of the flow profile for flow rates of 1μL/min, 5μL/min and 12μL/min, from top to bottom respectively. Here the molybdenum solution is replaced by water.

III

EVALUATION

6

Conclusion

In this thesis, an answer to the following research question was sought:

What is an accurate simulation model for the extraction process of technetium-99m and what are the optimized parameters for the geometrical design of the microfluidic platform to establish the highest possible extraction efficiency?

First, a literature study was performed from which insight is gained about the force balance which is present in the microchannel. The dimensionless Bond and Grashof number are used to analyze the gravity-to-surface tension ratio and the gravity-to-viscosity ratio. Consequently, it was concluded that surface tension and viscosity, on a microscale, have a more dominant influence on the flow profile than gravity forces. The force balance in the channel consists of the Laplace pressure and the hydrodynamic pressure difference.

$$\Delta p_{laplace} + \Delta p_{hyd} = 0 \tag{6.1}$$

The hydrodynamic pressure difference is a result of the pressure drop over each phase. The pressure drop depends on the flow rate, resistance and channel length. The pressure difference between the phases leads to a curvature of the interface, the curvature is defined by the contact angle. The Laplace pressure is initiated by the curved interface and operates in the opposite direction of the hydrodynamic pressure difference. When the hydrodynamic pressure difference exceeds the maximum Laplace pressure the interface will shift towards the channel wall. The maximum extraction length (L_{ext}) is derived using the maximum allowed hydrodynamic pressure difference and the Laplace pressure. An expression for the extraction length has been reported in research by Goyal and Desai [1]. However, comparing the current calculations with theirs, a miscalculation in their work was discovered. Consequently, the extraction length expression was adjusted. Furthermore, an adjustment is made in the expression for the resistance to make it more accurate for a two-phase system.

Also, the diffusion process of the technetium compound from the molybdenum solution to 2-butanone was analyzed. For the design of the diffusion model, interface phenomena have been taken into account. At the interface an immediate concentration equilibrium establishes. The interface concentrations are related to each other by the distribution coefficient K_D, which is a chemical property and depends on all substances present in the system. A numerical approach is used to simulate the diffusion process which can determine how the concentration profile evolves over time. The time is related to the spatial coordinate in the channel by the flow rate. This relation is used to calculated how much of the technetium compounds is diffused to 2-butanone during the contact time in the extraction channel.

In part II of this report the numerical and experimental simulation are described and the results are presented. The numerical simulation is based on the theory described in part I. The influence of variations of the geometrical parameters and flow rate on the extraction length was analyzed. It was shown that for a combination of low flow rates large channel width and large channel height the extraction length is the longest. A long extraction length is favorable since it creates a long contact time between the phases, which results in a large amount of extracted species. However the extraction length can not be infinitely long, the chip dimensions are approximately 2 cm by 5 cm, and generally the extraction length varies between 1 mm and 10 mm [1].

In subparagraph 5.1.3 the results for the optimization that is performed for the geometrical parameters and the flow rate are presented. For the optimization four test cases were proposed and executed. The variation of the parameters is conducted within the following ranges: w ranges from 10μm to 100μm, h ranges from 10μm to 100μm and Q_{aq} ranges from 10μL/min to 100μL/min. In the first test case, the highest possible extraction efficiency is sought. The extraction efficiency is calculated using equation 6.2.

$$Efficiency = \frac{\int_w^{2w} c(x)dx}{c_0(1-\frac{1}{1+K_d})w} * 100\% \tag{6.2}$$

This resulted in an extraction efficiency of 99% and the corresponding parameters are: w = 61.43μm, h=100μm, Q_{aq}=1.67$*10^-10m^3$/s, L_{ext}=12cm and t_{ext}=4.33s. The high efficiency is a consequence of the long extraction length. Within a time of 4.33 seconds the concentration profile has practically reached its equilibrium and almost all the technetium compounds are diffused to 2-butanone. However, an extraction length of 12 cm is not convenient for a microchip. The second test case also requests the highest possible efficiency but under the condition of a limited extraction length. The extraction length is not allowed to exceed the length of 1 cm. This resulted in an extraction efficiency of 64%. The corresponding parameters are: w = 22.86μm, h=100μm, Q_{aq}=1.67$*10^-10m^3$/s, L_{ext}=8.09mm and t_{ext}=0.11s. The extraction efficiency is decreased significantly due the limitation on the extraction length.

For the third and fourth test case the ranges for the flow rate and height are adjusted respectively. The flow rate range is adjusted to 20μL/min to 100μL/min and the height range is adjusted to 10μm to 50μm. During these test cases the condition of the limited extraction length still applied. The results show an even bigger decrease for the extraction efficiency: for the third test case the efficiency is decreased to 44%, in the fourth test case the efficiency is decreased to 27%.

From the test cases it can be concluded that an optimal extraction efficiency can be reached for a low flow rate, large channel width and height. However, the extraction length is too long to fit on a microchip. When the extraction length is limited the efficiency decreases significantly. Furthermore, when a higher flow rate and a smaller height is used the extraction efficiency decreases even further.

The experiment described in paragraph 5.2 studied the flow profile and interface stability of the combination of molybdenum solution and 2-butanone. It was observed that for relatively low flow rates, ranging from 5μL/min to 10μL/min, the interface is unstable and not located in the middle of the channel. For a flow rate of 20μm a more stable interface was observed and the interface was located in the middle of the channel. However, leakage is observed from the 2-butanone to the molybdenum solution. This can be a consequence of the fact that the geometrical parameters and flow rates were not adjusted to each other. Also, is it possible that the leakage is a consequence of the combination of a highly hydrophobic channel wall and aqueous solution. The aqueous solution feels a repulsive force from the wall, hereby creating space for 2-butanone to leak into the outlet channel. The experiment was repeated for the combination of 2-butanone and pure water. The results showed that 2-butanone and water do not create a stable interface. 2-Butanone interrupts the water flow, which can be due to the high solubility of 26% of 2-butanone in water.

From the experiment is can be concluded that the molybdenum solution and 2-butanone form an immiscible two-phase flow. However, a clean separation could not be established. The combination of water with 2-butanone does not create a immiscible two-phase flow and is therefore not suitable for the extractor.

To return to the research question, it can be confirmed that a simulation model is developed based on the theory described in part I. This model is generally applicable. However, if the extraction channel is not rectangular an adjustment must be made to the expression for the correction factor α, formulated in equation 2.7. The model is used to optimize the extraction efficiency by varying geometrical parameters and the flow rate. Hereby, the most optimal parameters are determined. Since both the force balance and the diffusion process greatly depend on the chemical properties of the substances present in the system, the accuracy of the model depends strongly on these properties. Since not all of the properties can be found in literature approximated values were used for some of the properties. This means that more accurate results can be established when these properties are obtained by future experimental research.

7

RECOMMENDATIONS

As mentioned throughout this paper, the model and optimization results are highly dependent on the chemical properties of the substances present in the system. Some of the properties can not be found in literature and should be determined by future experimental research. Before this model can be used as a design map for the extractor, the following properties should be determined: The interfacial tension between 2-butanone and the molybdenum solution (γ_{ab}), the advancing contact angle for the combination of 2-butanone, the molybdenum solution and PDMS (θ_{con}), the diffusion coefficient for pertechnetate in 2-butanone (D_b), the distribution coefficient for the combination of 2-butanone, the molybdenum solution and pertechnetate (K_D) and finally the viscosity of the molybdenum solution (μ_w). Hereby, the approximated values can be replaced and more reliable results will be obtained.

The optimum extraction efficiency of the extractor with an extraction length smaller than 1 cm is found to be 64%, within the given ranges of the geometrical parameters and flow rates. Without a limited extraction length an extraction efficiency of 99% can be achieved, as is shown in chapter 5. Without the option of altering the geometrical properties it might be possible to alter the chemical properties of the substances involved in the system. The extractor operates at room temperature and the values of the chemical properties are chosen for T=25° Celsius. However, when temperature is raised viscosities decrease and diffusion coefficients increase. Hence, if we want to accelerate the diffusion process we can raise the temperature of the molybdenum solution. This way, more pertechnetate can diffuse to 2-butanone within the contact time. Since the viscosities decrease when temperature is raised the pressure balance is influenced as well. It can be calculated and tested how the hydrodynamic pressure difference changes and how this will influence the extraction length. This is an idea worth investigating in future research.

Apart from the specific improvements of the extraction efficiency, research can be done on different designs for the extractor. Some studies are conducted on the so called *split-length design.*[19] This design consists of multiple extractor channels in series where the length of the individual segment can be taken smaller than the maximum extraction length. Hereby, the stability of the flow is better maintained while the total extraction length is longer. Figure 7.1 shows a schematic illustration of the split-length design. The same effect can be established when micropillars or partitions are placed at the interface of the extraction channel. In case this technique is used, the interface will attache to the pillars or partitions and the expression for the Laplace pressure has to be adjusted. A disadvantage of this technique is that the small sized features in the channel are challenging to fabricate.

Finally, during the experiments leakage from 2-butanone to the molybdenum solution was observed. The leakage can be a consequence of the hydrophobic channel wall and hydrophilic molybdenum solution. A solution to this problem could be to functionalize the channel walls. This means that the wall or specific parts of the wall are treated with a hydrophobic or hydrophilic coating. Using the right coating for the right

Figure 7.1: A schematic illustration of the split-length design of an extractor [1]

wall can result in repulsive and attracting forces on the flow in such a way that leakage can be overcome. How the walls should be functionalized in the case of the molybdenum solution, 2-butanone and PDMS could be analyzed by future experiments.

BIBLIOGRAPHY

[1] S. Goyal and D. V. Desai, *Thiolene and sifel-based microfluidic platforms for liquid-liquid extraction,* Chemical B: Sensors and Actuators **190**, 634 (2014).

[2] H. Bruus, *Theoretical microfluidics,* , Chapter 5 Diffusion (2008).

[3] *Down scaling of laboratory to a chip,* http://www.sle.sharp.co.uk/sharp/apps/sle-web/research/health_medical/index.html, accessed: 2015-06-22.

[4] *Chip,* http://www.fhcmi.org/LSE/Projects/08.html, accessed: 2015-06-22.

[5] M. W. L.P.B.M Janssen, *Transport phenomena data companion,* , Dimensionless Numbers p. 70 (2006).

[6] *Contact angle water and pdms,* http://www.rsc.org/suppdata/sm/c1/c1sm05574g/c1sm05574g.pdf, accessed: 2015-06-15.

[7] H. Bruus, *Theoretical microfluidics,* , Chapter 4 Hydraulic resistance and compliance (2008).

[8] F. Mortensen, N. S. Okkels and H. Bruus, *Reexamination of hagen-poiseuille flow: Shape dependence of the hydraulic resistance in microchannels,* Physical review E 71 (2005), 10.1103/PhysRevE.71.057301.

[9] K. Butt, H.J. Graf and M. Kappel, *Physics and chemistry of interfaces,* , Chapter 2 (2003).

[10] K. K. T. Aota, A. Mawatari, *Parallel multiphase microflows: fundamental physics, stabilization methods and applications,* The Royal Society of Chemistry **Lab Chip 9**, 2470 (2009).

[11] D. Lide, *Handbook of chemistry and physics,* (2004).

[12] M. Pohar, A. Lakner and I. Plazl, *Parallel flow of immiscible liquids in a microreactor: modeling and experimental study.* Microfluidics and Nanofluidics **12**, 307 (2012).

[13] H. van den Akker and R. Mudde, *Fysische transportverschijnselen,* , Chapter 4 Massatransport (2008).

[14] *Particles-diffusion,* http://www.arizersolovaporizer.com/how-does-diffusion-work/, accessed: 2015-06-21.

[15] H. van den Akker and R. Mudde, *Fysische transportverschijnselen,* , Chapter 3 Warmtetransport (2008).

[16] C. R. Kleijn and M. Rohde, *Stof overdracht door een fasegrensvlak,* Slides from the course Fysische Transportverschijnselen TN2785 (2015).

[17] G. H. Morris and H. Freiser, *Solvent extraction in analytical chemistry,* , Chapter 2 Principles of Solvent Exraction (1957).

[18] H. van den Akker and R. Mudde, *Fysische transportverschijnselen,* , Chapter 2 Mechanismen, kentallen en krahten (2008).

[19] F. Berthier, J. Van-Man Tran. Mittler and N. Sarrut, *The physics of a cowflow micro-extractor: Interface stability and optimal extraction length,* Sensors and Actuators A: Physical **149**, 56 (2009).

A

APPENDIX-A: MATLAB CODE FOR THE DIFFUSION SIMULATIONS

```
% specification of the variables %

Dw  = 1.48*10^-9; %m2/s diffusie coeffiecient in phase 1 (water)
Db  = 1.09*10^-9; % m2/s diffusie coefficient in phase 2 (butanone)
L   = 100*10^-6; % m
dt  = 0.00001; %s
dx  = 1*10^-6; %cm
t   = 1; % measurement time % voor t>6666.7 s doorverwarmingstheorie
m   = 1/778;
Cbb = 10^-6; % [mol/m^3] bulk concentratie in de waterfase op t=0
Cbw = 0;  % [mol/m^3] bulk concentratie in de butanone fase op t=0
Nt  = t/dt; % number of time steps
Nx  = L/dx; % 1/2*Nx is aantal stapjes voor Dw en Db

% epmty arrays creation (1x100) %
c  = zeros(1,Nx);
c2 = zeros(1,Nx);
x  = zeros(1,Nx);
D  = zeros(1,Nx);
AA = zeros(1,Nx);
BB = zeros(1,Nx);

% Diffusieconstanten ivullen
D(1:Nx/2)     = Dw;
D(Nx/2+1:end) = Db;

% Beginconcentraties %
c(1:Nx/2)     = Cbb;
c(Nx/2+1:end) = Cbw;

% AA en BB invullen %
for i=1:Nx
    AA(i)=1-(2*D(i)*dt)/(dx)^2;
    BB(i)=(D(i)*dt)/(dx)^2;
    if AA(i)<0 ;
        disp('oeps');
    end
end

% x vector maken %
x = (0:dx:L-dx) + dx/2;

%% Maak c2 (concentratie in volgende tijdstap)

for i=1:Nt
```

```
% Linker boundary conditie Db: flux door de wand op x = 0 is nul
c2(1) = c(1)*(AA(1)+BB(1)) + BB(1)*c(2);

% Rechter boundary conditie Dw: flux door de wand op x = L is nul
c2(Nx) = c(Nx)*(AA(Nx)+BB(Nx))+BB(Nx)*c(Nx-1);

% Interface conditions
c2(Nx/2) = (Db*c2(Nx/2+2)+Dw*c2(Nx/2-1))/(Db/m+Dw);
c2(Nx/2+1) = (Db*c2(Nx/2+2)+Dw*c2(Nx/2-1))/(Db+m*Dw);

% Concentratie profiel voor de rest van de celllen
c2(2:Nx/2-1)=c(2:Nx/2-1).*AA(2:Nx/2-1)+BB(2:Nx/2-1).*(c(1:Nx/2-2)+c(3:Nx/2));
%c(Nx/2)=grens concentratie in benzeen
c2(Nx/2+2:Nx-1)=c(Nx/2+2:Nx-1).*AA(Nx/2+2:Nx-1)+BB(Nx/2+2:Nx-1).*(c(Nx/2+1:Nx-2)+c(Nx/2+3:Nx));
%c(Nx/2+1) = grensconcentratie in water

c=c2; % ververs concentratieprofiel

% Gradient

GradCw=(c2(Nx/2)-c2(Nx/2-1))/(Nx/2-(Nx/2-1));
GradCb=(c2(Nx/2+1)-c2(Nx/2+2))/(Nx/2+1-(Nx/2+2));

con1 = GradCw*Dw; % con1=con2 namelijk de masse flux
con2 = GradCb*Db;

% hold on % om alle lijntje te plotten

c3=c(1:Nx/2);
c4=c(Nx/2+1:Nx);

C3=zeros(1,Nx);
C3(1:Nx/2)=c3;
C3(Nx/2+1:Nx)=NaN;

C4=zeros(1,Nx);
C4(1:Nx/2)=NaN;
C4(Nx/2+1:Nx)=c4;

end

figure(1);
plot(x,C3,'r:.',x,C4,'b:.');
xlabel('Position in the channel along the x-axis (m)','FontSize', 15); % x-axis label
ylabel('Concentration level (mol/m^3)','FontSize', 15); % y-axis label
h=legend('Concentration pertechnetate (Tc-99m compound) in the aqueous solution',
'Concentration pertechnetate (Tc-99m compound) in butanone (MEK)')
set(h,'FontSize',15)
xlim([0 L]); ylim([0 1.2*Cbb]);
k=title(['Concentration profile for the diffusing pertechnetate from the aqueous
phase to the butanone at time: ' num2str(i*dt) 's']);
set(k,'FontSize',15)
pause(0.01)

%% Calculations on the extraction efficiency %%

x1 = (0:dx:L/2-dx)+dx/2;
x2 = (L/2:dx:L-dx)+dx/2;


% Area under graph for bezeen and area under graph for water
Abezeen = trapz(x1,c3);
Awater  = trapz(x2,c4);

Coutw = Cbb*(L/2-dx)-Abezeen; % de verdwenen concentratie uit het water
Cinb  = Awater; % toegenomen concentratie in het butanone

Error = Coutw-Cinb % error in calculations doordat we een cel (dx) missen
```

B

APPENDIX-B: MATLAB CODE FOR THE OPTIMIZATION

```
clear; clc; close all; tic;
%% SETTINGS
hlim = [10 50]*1e-6;     % limits on channel height [m]
wlim = [10 100]*1e-6;    % limits on channel width [m]
Qlim = [20 100]*1e-6;    % limits on flow rate [L/min]
Qlim = Qlim/60*1e-3;     % [m^3/s]
N    = 15;                % number of steps in each optimization variable

Llim = 0.01;
Llimit = 1;

%% BRUTE FORCE OPTIMIZATION
h   = linspace(hlim(1),hlim(2),N);
w   = linspace(wlim(1),wlim(2),N);
Qaq = linspace(Qlim(1),Qlim(2),N);
[X,Y,Z] = meshgrid(h,w,Qaq);

f=zeros(N,N,N); Lext=f; t_ext=f; Cbut=f;

for i=1:N
    for j=1:N
        for k=1:N
            Lext(i,j,k) = PressureCalculation(h(i),w(j),Qaq(k));
            % Extraction length based on pressure balance
            %if Lext(i,j,k)>=0.05
                %f(i,j,k) = -1;  % Give configuration negative score because
                %it is too long
            %else
            t_ext(i,j,k) = Lext(i,j,k) / (Qaq(k)/(h(i)*w(j)));            % Diffusion time
            Cbut(i,j,k) = DiffusionEfficiency(w(j),t_ext(i,j,k));
            % Concentration transfer reached
            f(i,j,k) = Cbut(i,j,k); %Qaq(k); %^2 *(1/Lext); %(Cbut*Qaq(k)); % +
            %Cbut^2; %Cbb*(L/2-dx);
            % Configuration Score (mol/s transfer)
            %end
        end
    end

    % Show progress
    clc; disp(['Progress: ' num2str(round(i/N*100)) ...
    '% - Estimated time left: ' num2str(round(toc/(i/N)*(1-i/N))) ' seconds'])
    if i==N
        disp(['Finished after ' round(toc) ' seconds'])
    end
end
%%
```

```
if Llimit == true
    TooBig = find(Lext>=Llim);
    [hb,wb,Qb] = ind2sub(size(f),TooBig);
    f2=f;
    f2(hb,wb,Qb) = -1;
end

% Best = max(max(max(f)));
if Llimit==true
    Best=find(f2==max(f2(:)));
    [h1,w1,Q1] = ind2sub(size(f),Best);
    fBest = f2(h1,w1,Q1);
else
    Best=find(f2==max(f(:)));
    [h1,w1,Q1] = ind2sub(size(f),Best);
    fBest = f(h1,w1,Q1);
end

hBest = h(h1);
wBest = w(w1);
QBest = Qaq(Q1);

LBest=Lext(h1,w1,Q1);
tBest=t_ext(h1,w1,Q1);


disp(['Best result achieved: ' num2str(fBest*100) ' % efficiency'])
% disp(['Concentration out: ' num2str(CBest)])
disp('At: ')
disp(['Height:         ' num2str(hBest) ' m'])
disp(['Width:          ' num2str(wBest) ' m'])
disp(['Flow rate:      ' num2str(QBest) ' m^3/s'])
disp(['Channel Length: ' num2str(LBest) ' m'])

%% 3D CONTOUR PLOT
figure(1); clf;

Nplot = 100;
hq   = linspace(hlim(1),hlim(2),Nplot);
wq   = linspace(wlim(1),wlim(2),Nplot);
Qq = linspace(Qlim(1),Qlim(2),Nplot);
[Xq,Yq,Zq] = meshgrid(hq,wq,Qq);

fq = interp3(X,Y,Z,f2,Xq,Yq,Zq);

BestPlot=find(fq==max(fq(:)));
[h2,w2,Q2] = ind2sub(size(fq),BestPlot);
hold on
scatter3(wq(w2),hq(h2),Qq(Q2),'filled','m')

p = patch(isosurface(Xq,Yq,Zq,fq,0.10));   % Iso-surface of best 5% solutions
isonormals(Xq,Yq,Zq,fq,p)
p.FaceColor = 'green';
p.EdgeColor = 'none';

p2 = patch(isosurface(Xq,Yq,Zq,fq,0.08));   % Iso-surface of worst 5% solutions
isonormals(Xq,Yq,Zq,fq,p2)
p2.FaceColor = 'yellow';
p2.EdgeColor = 'none';

p2 = patch(isosurface(Xq,Yq,Zq,fq,0.05));   % Iso-surface of worst 5% solutions
isonormals(Xq,Yq,Zq,fq,p2)
p2.FaceColor = 'red';
p2.EdgeColor = 'none';

light('Position',[1 -1 1],'Style','local')

box on
title('The extraction efficiency for different paramater combinations','FontSize',15)
o=legend('Optimum','10% efficiency','8% efficiency','5% efficiency');
```

```
set(o,'FontSize',15)
ylabel('Height h','FontSize',15); xlabel('Width w','FontSize',15); zlabel
('Flow rate Q_{aq}','FontSize',15)
ylim([10 50]*1e-6);
view([-37.5+270 30])
zlim(Qlim)
```

```
function Cbut = DiffusionEfficiency(w,t_ext)
%% Settings
Dw  = 1.48*10^-9;   % m2/s diffusie coefficient in phase 1 (water)
Db  = 1.09*10^-9;   % m2/s diffusie coefficient in phase 2 (butanone)
L   = 2*w;          % m
m   = 1/778;        % Distributie coefficient
Cbb = 10^-6;        % [mol/m^3] bulk concentratie in de butanone fase op t=0
Cbw = 0;            % [mol/m^3] bulk concentratie in de waterfase op t=0

dt  = 1e-5;         % s
dx  = 1e-6;         % m
t_ext = round(t_ext,5); % Make time divisible by dt
L     = round(L,6);     % Make length divisible by dx
Nt  = round(t_ext/dt);  % number of time steps
Nx  = round(L/dx);      % 1/2*Nx is aantal stapjes voor Dw en Db
Int = round(Nx/2);      % Interface

%% CONCENTRATION PROFILE

% If extraction time or length is too short, skip and give diffusion value 0
if Nt <= 10 || Nx <= 10
    Cbut = 0;
else



% epmty arrays creation (1x100) %
c  = zeros(1,Nx);
c2 = zeros(1,Nx);
x  = zeros(1,Nx);
D  = zeros(1,Nx);
AA = zeros(1,Nx);
BB = zeros(1,Nx);

% Diffusieconstanten ivullen
D(1:Int)     = Dw;
D(Int+1:end) = Db;

% Beginconcentraties %
c(1:Int)     = Cbb;
c(Int+1:end) = Cbw;

% AA en BB invullen %
for i=1:Nx
    AA(i)=1-(2*D(i)*dt)/(dx)^2;
    BB(i)=(D(i)*dt)/(dx)^2;
    if AA(i)<0 ;
        error('AA<0');
    end
end

% x vector maken %
x = (0:dx:L-dx) + dx/2;

% Maak c2 (concentratie in volgende tijdstap)

for i=1:Nt
    % Linker boundary conditie Db: flux door de wand op x = 0 is nul
    c2(1) = c(1)*(AA(1)+BB(1)) + BB(1)*c(2);

    % Rechter boundary conditie Dw: flux door de wand op x = L is nul
    c2(Nx) = c(Nx)*(AA(Nx)+BB(Nx))+BB(Nx)*c(Nx-1);
```

```
    % Interface conditions
    c2(Int) = (Db*c2(Int+2)+Dw*c2(Int-1))/(Db/m+Dw);
    c2(Int+1) = (Db*c2(Int+2)+Dw*c2(Int-1))/(Db+m*Dw);

    % Concentratie profiel voor de rest van de celllen
    c2(2:Int-1)=c(2:Int-1).*AA(2:Int-1)+BB(2:Int-1).*(c(1:Int-2)+c(3:Int));
    %c(Int)=grens concentratie in benzeen
    c2(Int+2:Nx-1)=c(Int+2:Nx-1).*AA(Int+2:Nx-1)+BB(Int+2:Nx-1).*(c(Int+1:Nx-2)+c(Int+3:Nx));
    %c(Int+1) = grensconcentratie in water

    c=c2; % ververs concentratieprofiel

    % Gradient op de interface
    GradCw=(c2(Int)-c2(Int-1))/(Int-(Int-1));
    GradCb=(c2(Int+1)-c2(Int+2))/(Int+1-(Int+2));

    con1 = GradCw*Dw;
    % con1=con2, namelijk de masse flux phase 1 uit is gelijk aan de mass flux phase 2 in.
    con2 = GradCb*Db;

    c3=c(1:Int);
    c4=c(Int+1:Nx);

    C3=zeros(1,Nx);
    C3(1:Int)=c3;
    C3(Int+1:Nx)=NaN;

    C4=zeros(1,Nx);
    C4(1:Int)=NaN;
    C4(Int+1:Nx)=c4;
end
%%  CALCULATE DIFFUSION EFFICIENCY
x1 = 0:dx:(Int-1)*dx + dx/2;
x2 = Int*dx:dx:L-dx + dx/2;

% Area under graph for bezeen and area under graph for water
Awater = trapz(x1,c3);
Abutanone  = trapz(x2,c4);

Coutw = Cbb*(L/2-dx)-Awater; % de verdwenen concentratie uit het water
Cbut  = Abutanone/(Cbb*(L/2-dx)*(1-1/(1+1/m)));
% toegenomen concentratie in het butanone

end
end
```

```
function Lext = PressureCalculation(h,w,Qaq)
%% Variables
theta   = 108;
% (degree) contact angle (max contact angle for PDMS van literatuur)
y       = 48.2*10^-3;
% (N/m) interfacial tension for water and butanone (Y=Ywater-Ybutanone)
dx      = 0.1;                  %  x-stapjes
mu1     = 0.890*10^-3;          % (kg/s*m) viscousity in water
mu2     = 0.405*10^-3;          % (kg/m*s) viscousity in butanone
V_w     = Qaq/(w*h);            % (m/s) stroomsnelheid water
Q_b     = ((mu1/mu2)^0.76)*Qaq;
% (m^3/s) flowrate butanone (volgens conditie, interface in het midden)
V_b     = Q_b/(w*h);            % (m/s) stroomsnelheid butanone

Poutw   = 101325;               % (N/m^2) atmospheric pressure
Poutb   = 101325;
% (N/m^2) atmospheric pressure (als deze voor beide uitgangen gelijk zijn dan deltaPout = 0)

%% Pressure specification

PL     = (2*y*sind(theta-90))/h;              % Laplace pressure
```

```
PLad   = (2*y*sind(120-90))/h;                  % Advancing Laplace pressure
PLre   = (2*y*sind(90-90))/h;                   % Recedeing Laplace pressure

x       = 0:10^-5:30*10^-3;                     % x-axis
a       =((22/7)*(2*w+h)^2)/(w*h)-65/3;
% Part of resistance term (here Dh is taken to be 2w+2)
R_w     =(a*mu1*x)/(w*h)^2;                     % Resistance in water phase
R_b     =(a*mu2*x)/(w*h)^2;                     % Resistance in organic phase
Pw      = Qaq.*R_w;                             % drukval in waterfase
Pb      = Q_b.*R_b;                             % drukval in butanone fase
PH      = (Pw-Pb);                              % Hydrodynamic pressure


Lext=(h*PL)./((a*Qaq.*mu1)./(w^2*h)*(1-(mu2/mu1)^0.24)); % Extraction length
end
```